https://doi.org/10.5194/gchron-2021-24
Preprint. Discussion started: 20 August 2021

In situ produced cosmogenic krypton in zircon and its potential for Earth surface applications

Tibor J. Dunai [1*], Steven A. Binnie[1], Axel Gerdes[2]

[1] Institute of Geology and Mineralogy, University of Cologne, Zülpicher Str. 49b, 50674 Cologne, Germany.
[2] Institute for Geosciences, Goethe-University Frankfurt, Altenhöferallee 1, 60438 Frankfurt am Main, Germany.

Correspondence to: Tibor J. Dunai (tdunai@uni-koeln.de)

Abstract

Analysis of cosmogenic nuclides produced in surface rocks and sediments is a valuable tool for assessing rates of processes and the timing of events that shaped the Earth surface. The various nuclides that are used have specific advantages and limitations that depend on the time-range over which they are useful, the type of material they are produced in, and not least the feasibility of the analytical effort. Anticipating novel applications in Earth surface sciences, we develop in-situ produced terrestrial cosmogenic krypton (Kr_{it}) as a new tool; the motivation being the availability of six stable and one radioactive isotope (^{81}Kr, half-life 229 kyr) and of an extremely weathering-resistant target mineral (zircon). We provide proof of principle that terrestrial Kr_{it} can be quantified and used to unravel Earth surface processes.

1 Introduction

Cosmogenic nuclides have become an important tool to address questions in Earth surface sciences and paleoclimatology (Dunai, 2010; Gosse and Phillips, 2001; Balco, 2020). These nuclides are produced by particles of the cosmic ray cascade in the atmosphere and in minerals (i.e., in situ) at or close to the Earth's surface (Dunai, 2010; Gosse and Phillips, 2001). Each of the currently applied in-situ produced cosmogenic nuclides, i.e., ^{3}He, ^{10}Be, ^{14}C, ^{21}Ne, ^{26}Al, ^{36}Cl, and ^{53}Mn, has specific benefits and limitations that are rooted in its half-live, or stability in the case of ^{3}He and ^{21}Ne, the availability of suitable target minerals and our ability to measure the exceedingly low amounts produced (typically between 1-100 atoms per gram per year at sea level (Dunai, 2010)). In space, production rates are at least three orders of magnitude higher than on Earth at ground-level. Hence, many in-situ produced nuclides were initially developed in studies of extra-terrestrial material (e.g., meteorites, lunar rocks) some thirty years before they began to be used to transform quantitative Earth surface sciences. Cosmogenic krypton, $^{78,80\text{-}86}$Kr (Marti et al., 1966; Gilabert et al., 2002; Marti, 1967) has not made this transition yet, despite having the potential. Krypton is the only noble gas that has stable ($^{78,80,82\text{-}84,86}$Kr) and short-lived radioactive

https://doi.org/10.5194/gchron-2021-24
Preprint. Discussion started: 20 August 2021

isotopes (^{81,85}Kr) that are produced by cosmic rays (Gilabert et al., 2002; Marti et al., 1966). With a half-live ($T_{½}$) of 229 ± 11 kyr (Baglin, 2008), ^{81}Kr is particularly attractive for geomorphological applications, however, only the cosmogenic ^{81}Kr produced in the atmosphere has been used in Earth sciences to date, as a dating tool for old ice and groundwater (Buizert et al., 2014; Sturchio et al., 2004).

1.1 In situ produced *extra*-terrestrial krypton

In situ produced extra-terrestrial krypton, Kr_{iet}, in meteorites has been measured for over fifty years (Marti et al., 1966; Marti, 1967). For instance, the Kr-Kr dating method of meteorites (Marti, 1967) is routinely applied (e.g., Strashnov and Gilmour, 2013; Leya et al., 2015). All stable and moderately long-lived Krypton isotopes (including ^{85}Kr, $T_{½}$ = 10.7 yr, (Lerner, 1963)) are produced via spallation reactions (Gilabert et al., 2002) that are responsible for cosmogenic production. The main target elements for spallogenic Kr-production are Rb, Sr, Y, Zr and Nb (Gilabert et al., 2002; Marti et al., 1966; Leya et al., 2015), which have isotopes similar in mass (slightly higher masses) to Kr-isotopes. The minimum energies for neutrons producing Kr-isotopes by spallation from Zr are 50 - 100 MeV (higher end of range for isotope masses < 83 (Gilabert et al., 2002)).

1.2 In situ produced terrestrial krypton

In meteorites, Rb, Sr, Y, Zr and Nb are trace constituents at the ppm level (Mason et al., 1976; Leya et al., 2004). A key conceptual step in utilizing in situ produced terrestrial krypton, Kr_{it}, is the realization that, due to the geochemical differentiation of the Earth, the target elements for cosmogenic Kr form discrete minerals, or are enriched in other minerals. For example: Rb is enriched in biotite; Sr forms strontianite ($SrCO_3$), strontian calcite (up to several % Sr) or coelestine ($SrSO_4$); Y forms xenotime (YPO_4); Zr zircon ($ZrSiO_4$) and baddeleyite (ZrO_2); and Nb is present in columbite ($(Fe,Mn,Mg)Nb_2O_6$). Enrichments in these minerals over the concentrations in meteorites may be in the order of $10^3 – 10^4$, similar in magnitude to the cosmic ray flux differences between space and on Earth (Dunai, 2010), but in a reversed sense. The lower cosmic ray flux on Earth is thus fully compensated by the higher target-element concentrations and so determination of Kr_{it} in these minerals should be as easily attainable as Kr_{iet} is in meteorites.

Given the list of potential minerals, it appears that only zircon is near-ubiquitous on the Earth's surface, albeit as accessory mineral. Therefore, in the following we focus on zirconium as the target element and zircon as the target mineral. Considerations for other target elements/minerals are conceptually similar.

1.2.1 Spallation

As a first approximation of terrestrial production of krypton by spallation of zirconium due to neutrons we use thick target, 1600 MeV proton-irradiation experiments (Gilabert et al., 2002), and derive ^{83}Kr as

https://doi.org/10.5194/gchron-2021-24
Preprint. Discussion started: 20 August 2021

the most abundant Kr_{it}-isotope, followed by ^{82}Kr, ^{81}Kr, ^{80}Kr, ^{78}Kr, ^{84}Kr, ^{85}Kr and ^{86}Kr (1 : 0.81 : 0.67 : 0.58 : 0.29 : 0.22 : 0.005 : 0.004; for shielding depth ≥ 49.2 g/cm^2; Fig. 1).

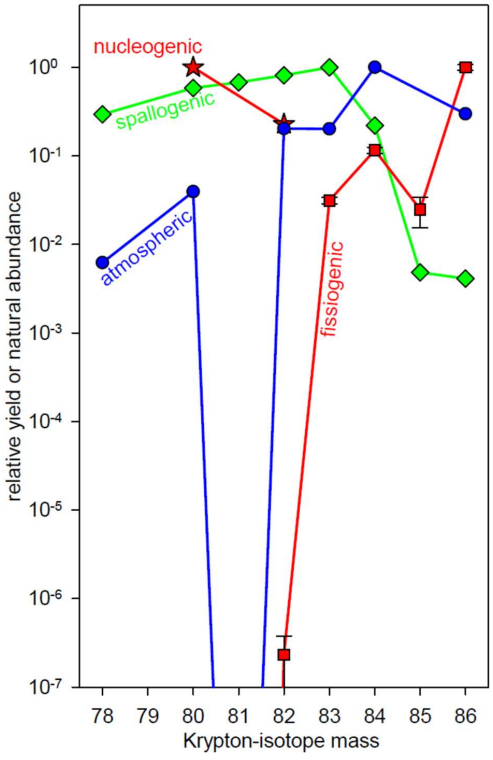

Fig. 1. Relative abundances of krypton isotopes in natural sources of krypton. Normalized krypton abundances (normalized to the most abundant isotope of a given source) of atmospheric (Aregbe et al., 1996; Sturchio et al., 2004), fissiogenic (from spontaneous fission of ^{238}U;(Jaea)), nucleogenic (thermal neutron capture by bromine; (Soppera et al., 2014; Kendrick, 2012)), and spallogenic (proton irradiation experiments, zirconium, ≥49 g cm-2 shielding; Table 2a of Gilabert et al., 2002) krypton. Most geological material on Earth contains atmospheric krypton, with all large geochemical reservoirs (i.e., mantle, crust) containing krypton of atmospheric composition.

The dominant reaction pathway for spallogenic Kr production on zircon appears to be of the type Zr(n,2α + xn)Kr (with neutron multiplicities x = 0, 1, 2, 3, 4, 5). This may be deduced from (i) the minimum energies required and (ii) the Zr- and spallogenic Kr-isotope abundances (Gilabert et al., 2002). At the low energy end (50 MeV (Gilabert et al., 2002)) only α-emissions are possible. This is due to the energy bonus of the emission of α-particles as compared the emission of individual nucleons, which is 28.3 MeV per α-particle (1), the separation energies of nucleons (neutrons and protons) requiring around 8.7 MeV in this mass range (Soppera et al., 2014) and protons additionally requiring > 8 MeV to overcome the Coulomb barrier. The most abundant spallogenic Kr-isotope ^{83}Kr may be

https://doi.org/10.5194/gchron-2021-24
Preprint. Discussion started: 20 August 2021

produced on the lightest and most abundant stable Zr-isotope ^{90}Zr (51.45%) via the energetically favourable (n, 2α) reaction, however, also on all other Zr-isotopes via (n, 2α + xn) reactions (x = 1,2,4,5). Kr-isotopes with masses smaller than 83 require in any case the additional separation of one or more neutrons, meaning higher minimum energies of the incoming neutrons are needed (Gilabert et al., 2002), which in turn explains the successively lower production as masses decrease. The lower production of ^{84}Kr is commensurate with the lower cumulative abundance of its target nuclides ^{91,92,94}Zr and, in the case of ^{92}Zr and ^{94}Zr, the requirement for the additional separation of one or two neutrons, respectively. The conspicuous relative rarity of spallogenic ^{86}Kr (Fig. 1), despite it being the Kr isotope closest in mass to Zr, probably stems from the fact that there is no (n, 2α + xn) pathway to produce it on stable Zr isotopes.

1.2.2 Negative muon capture

Muons (μ^-, μ^+), which are products from cosmic ray interactions in the Earth's atmosphere (Dunai, 2010; Stone et al., 1998) may also contribute to Kr production. Captured negative muons neutralize one proton and deliver 106 MeV (the mass of a muon at rest) to the nucleus (Dunai, 2010; Stone et al., 1998). Much of this energy is carried away by neutrino emission (ν_μ), such that on average close to 20 MeV are available for nuclear evaporation (Measday, 2001; Lifshitz and Singer, 1980). In the mass range of Zr-isotopes, captured negative neutrons may induce (μ^-, ν_μ + α) reactions with probabilities close to 10^{-4} (Wyttenbach et al., 1978). Production of krypton by muon capture on zirconium would require the separation of one additional charged particle, following reactions of the type (μ^-, ν_μ + 2αxn) and (μ^-, ν_μ + αpxn), with x = 0 to 4. The (μ^-, ν_μ + 2αxn) reaction would produce a radioactive Br-isotope decaying into a Kr-isotope. This would work for Kr-isotopes with mass ≤ 84, except for ^{81}Kr as it is shielded by stable ^{81}Br. Using the Coulomb-barrier reaction-probability relationship observed by Wyttenbach et al. (1978), we estimate that probabilities for (μ^-, ν_μ + αp) and (μ^-, ν_μ + 2α) reactions are at least 10^2 to 10^3 lower than a (μ^-, ν_μ + α) reaction for a given Zr-isotope. The required separation energy for emission of one or more neutrons (~ 8.7 MeV per neutron, see above) would decrease the likelihood of this even further (Lifshitz and Singer, 1980). Hence, the probability of negative muons captured by Zr-isotopes producing Kr-isotopes is smaller than 10^{-6}. Of muons coming to rest in zircon, 35 ± 4 % are captured by Zr (Von Egidy and Hartmann, 1982) and so the Kr-isotope yield from muon capture by Zr in zircon is less than 0.3 ppm. This translates into less than 10^{-6} atoms g^{-1} yr^{-1} at sea level and high latitude (Stone et al., 1998).

1.2.3 Interfering components

Geochemical components that may interfere with the analysis of cosmogenic krypton are the products of spontaneous fission of ^{238}U (fissiogenic krypton, Kr_{fis}) and neutron capture by bromine (nucleogenic krypton, Kr_{nuc}). These may become important when analysing U- or Br-rich minerals (Eikenberg et al.,

https://doi.org/10.5194/gchron-2021-24
Preprint. Discussion started: 20 August 2021

1993; Honda et al., 2004; Ruzie-Hamilton et al., 2016; Kendrick, 2012). Fission yields of krypton isotopes heavier than 81 atomic mass units (AMU) increase with increasing mass such that $^{86}Kr_{fis}$ is the most abundant, and the yield of $^{82}Kr_{fis}$ is negligible (Fig. 1; (Eikenberg et al., 1993; Jaea)). Spontaneous fission of ^{238}U does not produce Kr-isotopes lighter than 82 AMU. $^{80}Kr_{nuc}$ and $^{82}Kr_{nuc}$ may be produced by reactions on Bromine, $^{79}Br(n,\gamma)^{80}Kr$, $^{81}Br(n,\gamma)^{82}Kr$ (reaction cross sections for thermal neutrons are 10.32 and 2.36 barn, respectively (Soppera et al., 2014)). Bromine concentrations are low in silicate minerals (Kendrick, 2012; Ruzie-Hamilton et al., 2016; Teiber et al., 2015) but commonly not well constrained. The major geochemical reservoirs of Earth (e.g., mantle) contain krypton close to atmospheric composition (^{80}Kr 2.25%; ^{82}Kr 11.6%; ^{83}Kr 11.5%; ^{84}Kr 57.0%; ^{86}Kr 17.3%; ^{78}Kr 0.35%; ^{81}Kr 0.5 ppt; (Buizert et al., 2014; Aregbe et al., 1996)). Natural krypton is rarely measured in geological material due to the anticipated consistency of these values (Broadley et al., 2020; Trieloff et al., 2000).

1.2.4 Test of feasibility

To test the feasibility of using Kr_{it} for Earth surface science applications, we analysed a suite of zircon samples from near-surface sediment and bedrock with a wide range of anticipated exposure histories. The sediment samples are zircon megacrysts from kimberlitic, carbonatitic and metamorphic source rocks from locations in Australia (Mud Tank carbonatite; (Crohn and Moore, 1984; Currie et al., 1992)), Tanzania (Singida kimberlite field and Ubendian-Usagaran metamorphic belt (Mannard, 1962; Kabete et al., 2012)) and Germany (Ebersbrunn diatreme, Vogtland (Schmidt et al., 2013; Modalek et al., 2009)). The bedrock samples are from glacially scoured surfaces and a block from the Grimsel Pass, Switzerland (Wirsig et al., 2016). We use this suite of samples (see section 2 for details) to constrain terrestrial production ratios of Kr_{it}-isotopes, to cross-calibrate production rates with a well-established cosmogenic nuclide (^{10}Be), and to provide the first applications by constraining histories of burial and exposure in arid and temperate regions.

2. Sample materials

MUD: These zircons are from the Mud Tank carbonatite, Northern Territories, Australia (23°0'47"S; 134°16'45"E, 660 m) (32, 33, 83)(Crohn and Moore, 1984; Currie et al., 1992; Gain et al., 2019; Woodhead and Hergt, 2005). The carbonatite has a crystallization age of 731.0 ± 0.2 Myr (Gain et al., 2019), protracted cooling or a later thermal overprint during the Alice Springs Orogeny (450–300 Myr) is indicated by Pb-loss from some zircons (Gain et al., 2019). The emplacement occurred at temperatures ≤ 650 ºC, in a fluorine rich environment (Currie et al., 1992). Zircons from this location have a median Hf-concentration of 1.18 % (1st quartile 0.91%, 3nd quartile 1.19% (Woodhead and Hergt, 2005)). The two carbonatite bodies that constitute this occurrence rise about 10 m above the surrounding low-gradient landscape (Australian_Vermiculite_Industries, 2013). The elevation of possible sampling locations is 660 ± 5 m.

https://doi.org/10.5194/gchron-2021-24
Preprint. Discussion started: 20 August 2021

The material used in this study was obtained commercially via a private vendor, as part of two 1 kg batches of zircon sourced from an estate. The zircons were collected in the 1980s, when zircons were still abundant at the surface, prior to the Mud Tank becoming a well-frequented mineral collection site ('fossicking area'; (Australian_Vermiculite_Industries, 2013)). The zircons are sub-rounded, some show percussion marks from fluvial transport and fractured surfaces show signs of subsequent abrasion (Fig. 2). Most have a lighter colour than excavated zircons from the same site (the latter purchased from Dehne McLauchlin, Tasmania, Australia), suggesting bleaching from extended periods of exposure to sunlight (Gain et al., 2019). We assume that the zircons analysed were predominantly sampled from the surface. Individual zircons were crushed using a diamond mortar and subsequently sieved.

SING: These samples are from the Singida kimberlite field, Tansania (Mannard, 1962). The samples were obtained commercially (Mawingu Gems, Idar Oberstein, Germany). At least 54 diatremes (Mannard, 1962) occur in an area of about 1900 km^2 centred around 4°57'S, 34°25'E. The zircon-bearing kimberlites intruded into the Cretaceous African surface (Mannard, 1962; King, 1978) during the Eocene (Harrison et al., 2001) at an altitude ranging from 1100 to 1500 m (Harrison et al., 2001). We adopt an elevation of 1300 m for scaling, when comparing the results from Singida with other locations. The U-Pb ages of all (n=9) but one of the zircons used in this study are, within their individual uncertainties, identical to their mean age of 44.8 ± 0.2 Myr (±1SD; Table 2). One sample (SING-21) gives an age of 40.5±0.8 Myr (±1SD; Table 2). Remnants of the original tuff-rings are sometimes preserved (Harrison et al., 2001; Mannard, 1962) so the long-term erosion rates are presumably low. Much of the area is capped by relict calcretes and silcretes (Mannard, 1962). The area is covered by dry, deciduous woodland, currently receiving 520 ± 260 mm annual rainfall (Harrison et al., 2001; Mannard, 1962). Zircons are concentrated in river sands near the pipes (Mannard, 1962), where they are mined in small pits down to several metres depth. We assume such a source for our samples.

The individual 5 to 10 mm sized crystals (Fig. 2) are of gem quality. Their outsides show surface roughing and small percussion marks from fluvial transport. Their Hf-concentrations range between 0.6 and 1.1% (Table 2). Individual zircons were crushed using a diamond mortar and subsequently sieved.

RBM, GOEL & VOGT: These zircons stem from a kimberlitic diatreme near Ebersbrunn, Vogtland, Germany (Schmidt et al., 2013; Modalek et al., 2009). Ages of zircons from this location were determined as 71.1±0.8 Myr (U-Pb; Table 2), which we take as the intrusion age. The diatreme is located on a topographic saddle (450 m elevation) in a soil-mantled landscape of moderate relief. The diatreme was first inferred through geophysical surveys and subsequently confirmed via shallow drill cores (Schmidt et al., 2013).

Zircons were obtained from local collectors, either commercially from a private vendor (VOGT) or provided in exchange (RBM, GOEL; from Sven Kreher, Goldmuseum Buchwald, Germany). They were extracted from modern stream/river-bed sediments in the Göltzsch near Netschkau (VOGT; GOEL: 300 m, 50°37'25"N, 12°14'47"E), and its tributary Raumbach (RBM: 380 m, 50°37'0"N, 12°21'24"E). The

https://doi.org/10.5194/gchron-2021-24
Preprint. Discussion started: 20 August 2021

headwaters of the latter originate in the diatreme. The sampling site for RBM zircons is ~ 5 km downstream of the diatreme, those of VOGT and GOEL ~15 km. The smaller zircons (5-10 mm; all RBM and GOEL 1, 2 & 3) are mostly transparent, the pebble-sized zircons are opaque to translucent (all VOGT and GOEL 4 & 5; Fig. 2). Individual zircons were crushed using a diamond mortar and subsequently sieved.

SUM: These zircons are from the area around Sumbawanga, Tanzania (1850 m, 7°58'S, 31°37'E). The samples were obtained commercially (Mawingu Gems, Idar Oberstein, Germany). Potential source rocks are Paleoproterozoic metamorphic rocks (Kabete et al., 2012). We adopt an elevation of 1850 m for scaling but the actual elevation of the source and/or finding location may be higher. The samples exhibit signs of fluvial transport such as edge-rounding and percussion marks (Fig. 2). We assume that these samples were retrieved from stream sediments or sedimentary deposits. The samples are from two different batches (SUM 18 A & B; the other SUM 15 & 16) and possibly stem from different locations. Individual zircons were crushed using a diamond mortar and subsequently sieved.

GRIM: These samples (GRIM 19-1; GRIM 19-2; GRIM -1) are from Nägelisgrätli, east of Grimsel Pass, Switzerland. The Nägelisgrätli is part of the transfluence pass through which the last-glacial maximum Aare glacier was fed from the Rhône ice dome (Wirsig et al., 2016). ^{10}Be concentrations in quartz-samples from the Nägelisgrätli are consistent with a single stage exposure history, with complete resetting of signals of prior exposure via glacial erosion (Wirsig et al., 2016). The Grimsel Granodiorite (part of the Central Aar Granite) has an intrusion age of 298±2Ma (Schaltegger and Corfu, 1992) and was subsequently affected by regional metamorphism during the Alpine orogenesis around 30–35 Myr ago (Hettmann et al., 2009).

Samples for the current study were taken at 2390 m (GRIM 19-1: 46°33’57.66”N, 8°20’46.57”E; GRIM 19-2: 46°33’57.58”N, 8°20’46.71”E) and 2478 m (GRIM-1: 46°34’13.9”N, 8°21’6.4"E) elevation. GRIM-1 and GRIM 19-1 are bedrock samples (Fig. 3). GRIM 19-2 a loose block in a shallow depression (Fig. 3) and was presumably ice-transported to this location, as all other means of transport, such as falling or rolling from uphill, can be excluded. The topography in the immediate vicinity of the sampling sites is favourable for accumulating significant snow cover (significant in terms of capability to reduce cosmogenic nuclide production). We performed no snow-cover corrections, since the main purpose of these samples is to cross-calibrate production rates of cosmogenic nuclides that are equally affected by snow-cover, i.e., snow-cover effects cancel each other out. The same applies to topographic shielding corrections, which we likewise did not apply. Electro pulse disaggregation of samples and subsequent zircon separation, by standard magnetic and heavy liquid techniques, was conducted by Zirchron LLC, Tucson, Arizona, USA. The zircon grains are < 125 microns (Fig. 2).

https://doi.org/10.5194/gchron-2021-24
Preprint. Discussion started: 20 August 2021

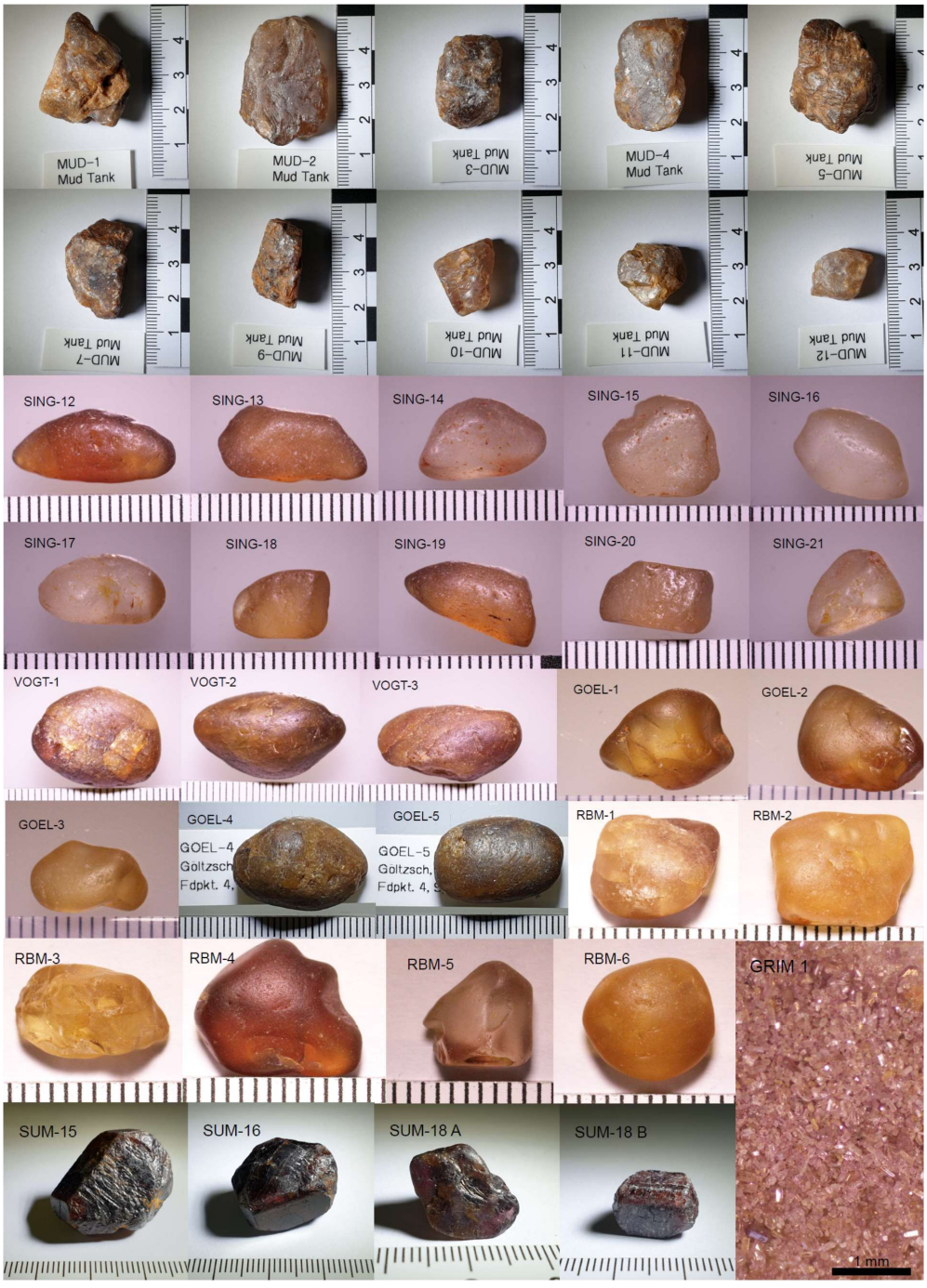

Figure 2: Photos of the zircons investigated. Scales are mm and cm. GRIM-1 is exemplary also for samples GRIM 19-1 and GRIM 19-2 (not shown). Crystals' weights are provided in Table 1 (where applicable).

https://doi.org/10.5194/gchron-2021-24
Preprint. Discussion started: 20 August 2021

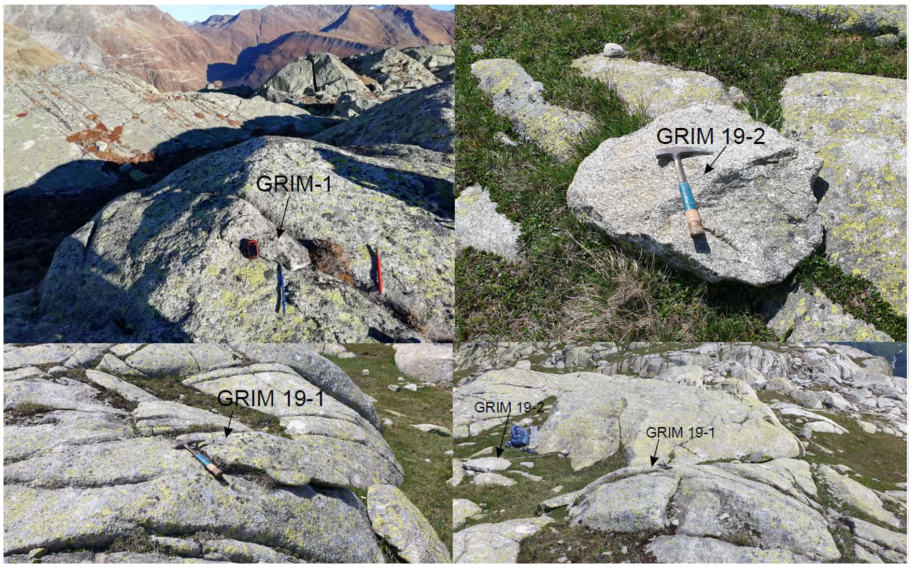

Figure 3: Samples and sampling locations on the Näglisgrätli, Grimsel Pass, Switzerland. Photo of GRIM 1 by P. Abbott/ G. King; all others T. Dunai.

3 Methods

3.1 Krypton isotope determinations

The general layout of the noble gas set-up at Cologne is described in Ritter et al. (2021), who focus on the analysis of cosmogenic neon. Here we reproduce some aspects of this description (Ritter et al., 2021), adding details that are pertinent for Kr-extraction from zircon and cosmogenic Kr-analysis.

3.1.1 Krypton extraction from zircon

Samples are placed into tantalum tubes (4 mm outer diameter, ca. 12 mm long) that are pinched off at both ends. The tantalum tubes are placed into tungsten cups, which in turn are placed into a molybdenum sample revolver. For thermal insulation, several fragments (250-500 micron) of zirconia (cubic stabilized zirconium oxide, melting point ~2700°C) are placed between the cups and revolver. Energy for the heat-extraction in vacuum is provided by an output-tuneable 600 W fiberlaser (Rofin StarFiber600) at 1064nm wavelength through galvanometer scanner optics (Rofin RS S 14 163/67 0°), a UV-grade fused silica viewport (MDC Precision, 9722005) and a single-use fused-silica protective glass (Thorlabs, WG41050). The tantalum-tubes are heated via scanning a continuous wave beam with 200W power for a total of five minutes. The scanning speed is 20 cm/s; first rastering a rectangular area of 4 by 10 mm with a defocussed beam (~ 0.5 mm diameter) for three minutes, then with focussed beam a circular area with 5 mm diameter, on the then shrivelled tube, for two minutes. The temperature achieved is sufficient to melt the top of the Tantalum tube (melting point of Tantalum is 3020 ± 15 °C; (Arblaster, 2018)) and to quantitatively sublimate the silica content of zircon. Zircon melts

https://doi.org/10.5194/gchron-2021-24
Preprint. Discussion started: 20 August 2021

incongruently above ~1690°C (Kaiser et al., 2008) and the silica is presumably lost as silicon monoxide and oxygen (Fig. 4; Schick, 1960). Silicon monoxide is observed as brown coating on the protection windows; the coating starts to appear within about one minute after starting the laser extraction. The quantitative loss of silica is verified by weighing of the tantalum tubes after heat-extraction; in most cases, the measured loss indicates also partial sublimation of ZrO_2 (Fig. 5; Hoch et al., 1954).

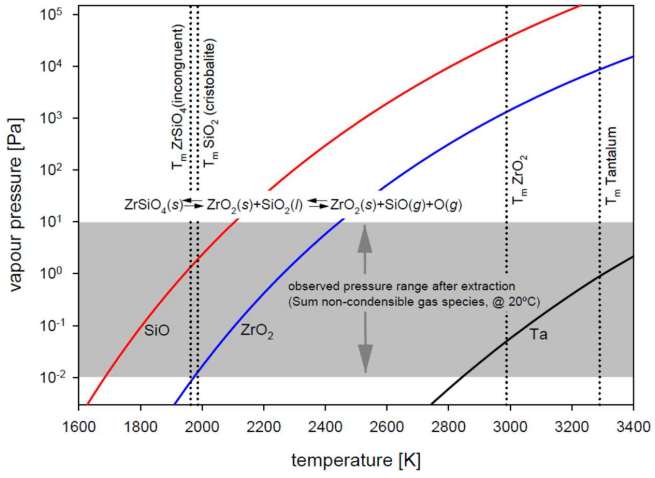

Figure 4: Vapour pressure of Silicon monoxide (SiO), zirconia (ZrO_2) and tantalum (Ta) as a function of temperature (Schick, 1960; Hoch et al., 1954; Arblaster, 2018; Kaiser et al., 2008), and the melting points of zircon ($ZrSiO_4$), cristobalite (SiO_2) and zirconia (Kaiser et al., 2008). Zircon melts incongruently to ZrO_2 and SiO_2-melt (the melting temperature of the high-temperature modification of SiO_2, cristobalite, is only ~10K higher than that of zircon) (Kaiser et al., 2008). At a given temperature the vapour pressure of SiO is one to two orders of magnitude higher than that of ZrO_2, the larger differences are at lower temperatures. Above the melting point of cristobalite, SiO can boil off, rather than sublimate from the surface of a solid (as is the case for ZrO_2, below its melting point), if the pressure in the extraction cell is lower than the vapour pressure. Observations of the residual pressure of non-condensible gases after extraction (at this time the laser furnace is still hot from the extraction, but the laser power is switched off) indicate that in our experimental setup SiO may boil off at temperatures > 2100K. The higher vapour pressure and the ability to boil off from a liquid leads to a preferential loss of SiO, as compared to ZrO_2, from zircon at high temperatures.

https://doi.org/10.5194/gchron-2021-24
Preprint. Discussion started: 20 August 2021

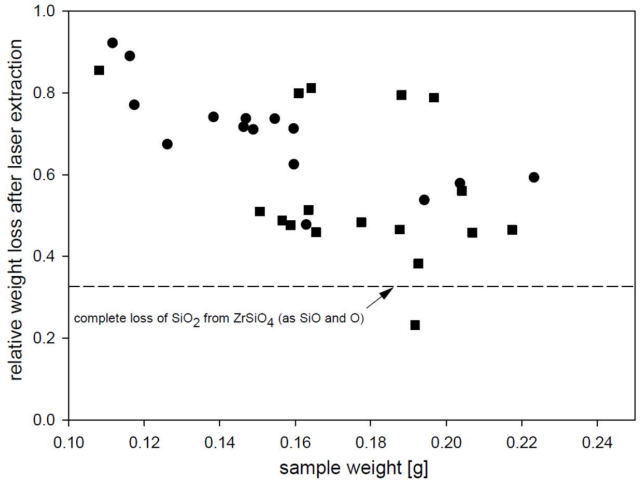

Figure 5: Relative mass loss of zircon samples after laser extraction as a function of initial sample weight. Squares denote samples with grain sizes above 125 µm, circles denote samples that (also) contain grains smaller 125 µm. All but one sample (RBM-6) have completely lost their constituent SiO_2 and some of the ZrO_2 residue (see also Fig. 4).

3.1.2 Krypton isotope determination

Subsequent to the extraction, the evolved gases cleaned by sequential exposure to two reactive metal getters (SAES NP50) and a stainless steel watertrap (held at 205 K). The noble gases are separated cryogenically on a stainless steel coldtrap (Janis, twin coldhead model 204): neon and heavier noble gases are quantitively condensed on the trap at 24 K; the trap is then heated to 120 K and pumped (neon and argon are removed; >99% of Kr remains on the trap); finally, the trap is heated to 240 K to release Kr for analysis in a noble gas mass spectrometer.

The noble gas mass spectrometer (Helix MCPlus, Thermo Fisher Scientific) is equipped with five Combined Faraday Multiplier modules (CFM). One CFM is fixed in axial position (Ax) and two movable CFM are each on the low (L1, L2) and the high (H1, H2) mass side of Ax. The L1 CFM is flipped as compared to the factory-standard configuration (lateral positions of multiplier and faraday slits are swapped). Four Faraday collectors are fitted with 10^{13} Ω pre-amplification resistors (H1, Ax, L1, L2), one with 10^{12} Ω (H2). The multipliers are operated in ion-counting mode. One CFM module (L1 position) has a higher resolution (0.3 mm entry slit), the others have regular resolution (0.6 mm slits). At the operation conditions we used for krypton analysis (source slit 0.25 mm; 10 KV acceleration voltage), mass resolution (at 5% peak valley) and mass resolving power (between 10% and 90% of peak) on the L1 detector with 0.3 mm collector slit width are ~1700 and ~6500, respectively. For the detectors with 0.6 mm collector slit, the corresponding values are ~1000 and ~6000, respectively. This resolution allows the full separation of krypton isotopes from hydrocarbon isobars (~600 is required; Burnard et al., 2013). The resolution of the L1 detector achieves separation of $^{40}Ar_2H^+$ from $^{81}Kr+$ at

https://doi.org/10.5194/gchron-2021-24
Preprint. Discussion started: 20 August 2021

$^{81}Kr^+$-peak centre. Partial resolution is achieved on the remaining detectors, permitting interference-free ($^{40}Ar_2H^+$) analysis of $^{81}Kr^+$ in an off-centre position. Interference of $^{80}KrH^+$ on $^{81}Kr^+$ cannot be resolved; we determine the $^{84}KrH^+/^{84}Kr^+$-ratio during calibration gas measurements (observed range 2 - 5 x 10^{-6}; n=26) as a proxy for the $^{80}KrH^+/^{80}Kr^+$-ratio and correct sample signals accordingly. Likewise, the interference from $^{81}Br^+$ cannot be resolved, we corrected it via monitoring and subtracting the background at the position of $^{81}Kr^+$ during blank measurements. This background was found to be stable at the equivalent of 2200 ± 200 (n=7; 1SD) atoms ^{81}Kr. Using multiples (m) of the blank value (2200 ± 200 atoms), we estimate the detection limit for ^{81}Kr with the current setup is ~ 7000 atoms (m=3). Blanks yield 0.65±0.30 attomol ^{84}Kr (n=8). Measurements of hot blanks 0.75±0.25 attomol ^{84}Kr (hot laser extraction, n=5, 1SD of mean), cold blanks 0.55±0.05 attomol ^{84}Kr (same volume, but laser power off, n=2, 1SD of mean), or the line blank 0.5±0.1 attomol ^{84}Kr (purification line only, without the laser extraction volume, n=1, 1SD of measurement) are indistinguishable from each other. The observed Kr-blanks are about four-times lower than the lowest reported previously (Zimmermann et al., 2018).

We analysed the krypton isotopic abundances in multicollection mode. First, masses 78 to 85 are measured in four cycles on the multipliers; 1st: ^{84}Kr(H2), ^{83}Kr(H1), ^{81}Kr(Ax), ^{80}Kr(L1), ^{78}Kr(L2); 2nd: ^{83}Kr(H2), ^{82}Kr(H1); 3rd: ^{82}Kr(Ax), ^{81}Kr(L1); 4th: $^{84}KrH^+$(H2), ^{84}Kr(H1), followed by sequential analysis of masses 86, 84, 83 and 82 on the axial Faraday cup. Gain calibrations of multipliers are performed relative to the H1 multiplier, using the measurements of calibration gas (air-pipette, containing 11.25±0.01 fmol Kr) and the isotopic composition of air (Aregbe et al., 1996). The gain of the H1 multiplier is in turn calibrated to the axial Faraday collector using the corresponding $^{84}Kr^+$ readings of calibration gas measurements. Within each of the two measurement periods, the variability of ^{84}Kr Faraday signals for calibration gas were smaller than ± 1% (1 SD, n=26). Between the two periods the ion source was switched off and after turning the source back on the sensitivity had dropped by 4%. Calibration gas was measured prior to a set of two or three sample measurements on a given day, with these preceding calibrations used for gain calibration and interference correction ($^{80}KrH^+$) of the subsequent samples. We use both determinations of ^{81}Kr, on Ax (off-centre) and on L1, to obtain an error weighted mean of intensities. We calculate the concentration of $^{78}Kr_{it}$ from the measured $^{78}Kr/^{82}Kr$ ratio, assuming that all ^{82}Kr is atmospheric. The $^{81}Kr_{it}$ concentration is corrected for interferences ($^{81}Br^+$, $^{80}KrH^+$).

3.2 ^{10}Be determination

Samples were ground and sieved to 250-1000 µm and subsequently purified through sequential HF-leaching (Kohl and Nishiizumi, 1992). ICP-OES was used to verify the purity of the quartz before dissolution. ^{10}Be AMS (Accelerator Mass Spectrometry) targets were prepared using the stacked column approach (Binnie et al., 2015). A reagent blank and in-house quartz reference material (CoQtz-N;

https://doi.org/10.5194/gchron-2021-24
Preprint. Discussion started: 20 August 2021

(Binnie et al., 2019)) was prepared in tandem with the samples. AMS measurements were made on CologneAMS (Dewald et al., 2013), normalized to the ICN standard dilutions prepared by Nishiizumi for ^{10}Be (Nishiizumi et al., 2007). Concentrations of ^{10}Be are reported following blank subtractions, which were less than 1% of the total number of nuclides measured. The 1 standard deviation analytical precision of the nuclide concentrations was estimated by summing in quadrature the relative uncertainties on the AMS measurements, both the samples and the blank, along with a 1% (1 SD) estimate for the precision of the mass of ^{9}Be added during spiking. Concentrations obtained from intercomparison material (CoQtz-N; (Binnie et al., 2019)) measured alongside the samples are consistent with the long-term arithmetic mean 2.43 ± 0.11 x 10^6 atoms g^{-1} CoQtz (1SD; N = 55) at our laboratory.

3.3 U-Pb-age determination

U, Th and Pb isotopes of zircon were performed by LA-ICPMS at FIERCE (Frankfurt Element and Isotope Research Center), Goethe University Frankfurt following the methods described in Gerdes et al. (2009). A Thermo Scientific Element XR sector field ICP-MS was coupled to a RESOlution 193 nm ArF Excimer laser (Compex Pro 102, Coherent) equipped with an S-155 two-volume ablation cell (Laurin Technic, Australia). The GJ-1 zircon (603 ± 1 Myr) was used as primary zircon reference material (RM) and RMs BB-16, Plešovice and Monastery zircon for validation of the analytical results. The results obtained on these zircon RMs were within 0.8% or better of the reported ages. Data processing (including common lead correction) was performed using an Isoplot (Ludwig, 2012)-supported Microsoft Excel-based spreadsheet (Gerdes and Zeh, 2009). Uncertainties reported are at the 2SD level (i.e. 95% confidence) and are calculated by quadratic addition of the internal uncertainties (SE), counting statistics, gas-background uncertainties, common Pb corrections, the excess of scatter derived from the primary RM.

4 Results

The results of the, Kr-isotope determinations, U-Pb age-determinations, and the ^{10}Be-results are provided in Tables 1, 2 and 3, respectively.

https://doi.org/10.5194/gchron-2021-24
Preprint. Discussion started: 20 August 2021

SampleD	weight crystal [g]	grain size§ [µm]	weight analysed [mg]	$^{84}Kr/^{82}Kr$	$^{83}Kr/^{82}Kr$	$^{80}Kr/^{82}Kr$	$^{78}Kr/^{82}Kr$	^{82}Kr [10^6 g^{-1}]	^{81}Kr [10^6 g^{-1}]	$^{78}Kr_{cos}$ [10^6 g^{-1}]
SING-12	1.42	75-250	162.9	4.475(19)	0.9855(39)	0.2124(10)	0.04087(28)	96.0(1.1)	1.03(3)	4.40(13)
SING-13	1.40	75-250	133.8	4.269(15)	0.9974(28)	0.2315(11)	0.04997(45)	85.7(1.1)	3.62(6)	7.08(19)
SING 14	1.21	75-250	116.2	4.496(13)	0.9825(22)	0.2400(12)	0.04126(41)	99.7(1.2)	2.69(6)	4.77(19)
SING-15	1.44	75-250	138.4	4.051(18)	0.9942(40)	0.2348(12)	0.05607(37)	69.7(7)	2.83(4)	7.19(12)
SING-16	1.19	75-250	111.6	3.952(14)	0.9733(26)	0.2373(13)	0.05640(42)	67.0(8)	0.626(41)	6.82(13)
SING-17	1.31	75-250	146.3	4.357(21)	0.9813(41)	0.2117(11)	0.04326(35)	78.2(8)	2.12(4)	4.31(13)
SING-18	0.91	75-250	126.2	4.415(24)	0.9767(50)	0.2113(14)	0.04079(45)	52.8(8)	0.152(30)	2.37(11)
SING-19	1.37	75-250	159.7	4.209(15)	0.9914(30)	0.2253(13)	0.05046(45)	59.9(8)	2.27(4)	5.00(13)
SING-20	1.35	75-250	159.6	4.335(22)	0.9830(49)	0.2166(13)	0.04470(53)	58.2(7)	0.154(26)	3.55(14)
SING-21	1.01	75-250	117.4	4.538(24)	0.9593(49)	0.1916(14)	0.03180(32)	74.3(9)	0.390(26)	0.40(11)
VOGT-1	7.75	125-250	199.8	3.903(27)	0.9826(65)	0.2377(19)	0.05671(48)	49.9(7)	0.267(19)	5.08(11)
VOGT-2	7.43	125-250	192.7	3.216(12)	1.0755(38)	0.3156(18)	0.09928(67)	53.6(1.0)	0.215(20)	11.8(2)
VOGT-3	4.49	125-250	156.5	3.561(13)	1.0688(32)	0.2964(14)	0.08662(53)	61.6(8)	0.271(22)	12.3(2)
GOEL-1	1.33	125-250	165.5	3.460(19)	1.0501(55)	0.2947(19)	0.08625(65)	63.8(9)	0.246(25)	12.3(2)
GOEL-2	1.60	125-250	160.9	4.189(18)	1.0030(41)	0.2360(13)	0.05380(62)	61.8(8)	0.205(27)	6.00(17)
GOEL-3	0.62	125-250	108.0	4.317(36)	0.9880(16)	0.2824(19)	0.04749(59)	103(2)	0.483(46)	7.51(28)
GOEL-4	8.11	125-250	214.5	4.047(17)	1.0178(40)	0.2437(12)	0.06067(58)	61.9(8)	0.270(21)	7.53(17)
GOEL-5	7.56	125-250	211.1	4.110(14)	1.0137(28)	0.2411(10)	0.05815(33)	92.4(1.2)	0.244(18)	10.5(2)
RBM-1	1.23	125-250	206.9	3.565(13)	1.0237(27)	0.2826(14)	0.08023(47)	94.5(1.2)	0.438(20)	16.7(3)
RBM-2	1.86	125-250	150.6	3.937(18)	1.0016(42)	0.2444(14)	0.06005(42)	63.5(7)	0.329(22)	7.36(12)
RBM-3	0.90	125-250	217.5	4.507(19)	0.9723(38)	0.2016(11)	0.03545(37)	60.3(6)	0.521(17)	1.31(10)
RBM-4	1.32	125-250	187.7	4.842(21)	1.0651(44)	0.2080(13)	0.05148(38)	65.6(1.0)	0.430(25)	6.62(15)
RBM-5	0.72	125-250	177.5	4.253(16)	1.0071(33)	0.2338(11)	0.05189(31)	98.8(1.4)	0.423(22)	8.93(18)
RBM-6	1.04	125-250	191.8	4.254(14)	1.0103(30)	0.2377(09)	0.05343(27)	157(2)	0.386(17)	15.3(2)
MUD-1	25.4	125-250	196.7	4.475(15)	0.9652(30)	0.2054(10)	0.03532(24)	56.5(7)	1.65(3)	1.19(6)
MUD-2	22.6	125-250	207.3	4.249(22)	0.9734(47)	0.2123(12)	0.04371(33)	64.7(7)	1.53(2)	3.60(10)
MUD-3	16.4	125-250	164.2	4.541(14)	0.9705(28)	0.2290(19)	0.03461(19)	59.9(7)	1.45(3)	1.08(5)
MUD-4	25.7	125-250	189.4	4.285(16)	0.9805(31)	0.2170(10)	0.04347(42)	63.7(7)	2.38(4)	3.51(12)
MUD-6	30.9	125-250	232.7	4.496(18)	0.9851(37)	0.2074(10)	0.03903(28)	80.8(8)	1.57(2)	3.06(11)
MUD-7	17.6	125-250	188.2	4.649(15)	0.9895(29)	0.2539(19)	0.03595(59)	91.3(1.1)	1.81(4)	2.26(25)
MUD-9	13	125-250	204.1	4.429(19)	0.9797(35)	0.2064(11)	0.03866(40)	68.6(8)	2.13(4)	2.44(12)
MUD-10	9.68	125-250	202.4	4.352(23)	0.9804(49)	0.2094(14)	0.04131(32)	65.2(6)	2.22(3)	3.03(10)
MUD-11	11.0	125-250	205.1	4.530(25)	0.9728(53)	0.1996(13)	0.03438(28)	54.5(6)	1.37(2)	0.93(7)
MUD-12	8.00	125-250	220.3	4.461(13)	0.9856(27)	0.2141(09)	0.04014(25)	99.1(1.2)	1.83(3)	4.21(12)
SUM-15	20.9	125-250	177.2	4.672(21)	1.0477(45)	0.2062(15)	0.03903(36)	48.7(7)	1.16(3)	1.91(9)
SUM-16	16.2	125-250	150.3	4.621(36)	1.0479(78)	0.2098(18)	0.04049(59)	44.5(6)	2.12(4)	2.03(12)
SUM-18A	3.08	125-250	158.8	4.612(19)	0.9816(37)	0.1933(10)	0.03242(47)	60.5(8)	1.48(4)	0.50(13)
SUM-18B	2.42	125-250	163.5	4.648(13)	0.9910(21)	0.2019(09)	0.03313(31)	79.7(9)	0.528(23)	0.93(12)
GRIM-1	n.a.	<125	223.3	5.110(28)	1.1300(57)	0.2025(14)	0.03159(38)	55.7(7)	0.482(20)	0.27(11)
GRIM-19-1A	n.a.	<125	203.7	5.097(28)	1.1121(59)	0.1985(12)	0.03158(25)	66.5(9)	0.445(19)	0.33(8)
GRIM-19-1B	n.a.	<125	194.2	5.011(26)	1.0860(52)	0.1975(13)	0.03109(37)	75.3(1.0)	0.480(19)	0.18(14)
GRIM-19-1C	n.a.	<125	148.9	5.091(12)	1.1084(23)	0.2033(07)	0.03177(31)	48.9(6)	0.462(27)	0.29(8)
GRIM-19-2A	n.a.	<125	154.6	5.053(23)	1.0996(46)	0.1975(12)	0.03135(30)	58.8(7)	0.424(26)	0.22(9)
GRIM-19-2B	n.a.	<125	146.9	5.080(20)	1.0980(42)	0.2019(11)	0.03141(20)	59.8(7)	0.415(26)	0.24(6)

Table 1: The analytical uncertainties of the isotope ratios and abundances are 1SD, they are provided in brackets as last significant digits. $^{78}Kr_{cos}$ is calculated from the difference between the measured and the atmospheric $^{78}Kr/^{82}Kr$-ratio (Aregbe et al. 1996). §grain size after crushing and sieving. GRIM-19-1A, -1B, and -1C are aliquots of sample GRIM-19-1; GRIM-19-2A and -2B are aliquots of sample GRIM-19-2.

https://doi.org/10.5194/gchron-2021-24
Preprint. Discussion started: 20 August 2021

Sample ID	U-Pb age [Myr]	Hf [ppm]
SING-12	45.14 ± 1.08	6980 ± 130 (n=6)
SING-13	45.14 ± 1.07	6870 ± 160 (n=7)
SING 14	44.86 ± 1.23	8760 ± 150 (n=7)
SING-15	44.86 ± 1.38	10200 ± 230 (n=6)
SING-16	44.83 ± 1.17	8010 ± 150 (n=6)
SING-17	44.36 ± 1.27	8650 ± 120 (n=6)
SING-18	44.70 ± 0.35	7870 ± 140 (n=6)
SING-19	44.80 ± 0.31	6410 ± 94 (n=6)
SING-20	44.51 ± 0.34	7960 ± 100 (n=6)
SING-21	40.47 ± 0.42	10810 ± 160 (n=7)
Göltzsch (zr1-4)	71.2±0.8	n.d.

Table 2: Laserablation ICP-MS age-determinations and Hf-concentrations of zircons from Singida, Tansania (samples 'SING'), and the Vogtland ('Göltsch (zr1-4)', mean age of four zircons from the same locality as samples 'VOGT' and 'GOEL'). The mean age of the samples from Singida is 44.80±0.24 Myr (1SD; n=9; SIN-21 excluded). Within their individual uncertainties, the individual ages of all zircons, bar SING-21, agree with this mean. The age of SING-21 is significantly (>3SD) lower than this mean. The numbers in brackets denote the number of analyses from which the mean Hf-concentration was calculated.

Sample	AMS ID	Lab ID	$^{10}Be/^{9}Be$	^{10}Be concentration [10^5 atoms/g]
GRIM-1	s16545	KL-1122B	$4.03 \pm 0.13 \times 10^{-13}$	3.21 ± 0.11
GRIM-19-1	s16546	KL-1123B	$3.63 \pm 0.12 \times 10^{-13}$	3.07 ± 0.11
GRIM-19-2a	s16547	KL-1124B	$3.03 \pm 0.11 \times 10^{-13}$	2.44 ± 0.09
GRIM-19-2b	s16548	KL-1125B	$3.48 \pm 0.12 \times 10^{-13}$	2.48 ± 0.09
chemistry blank	s16550	KL-B14B	$9.8 \pm 3.3 \times 10^{-16}$	n.a.

Table 3: ^{10}Be results for quartz samples from the Grimsel Pass, Switzerland. GRIM-19-2a and GRIM-19-2b are duplicate measurements sample GRIM-19-2. The uncertainties denote the standard deviation (1SD). 10Be concentrations are reported after the chemistry blank correction. Samples, 24.03 to 28.33 g quartz, were spiked with 300µg Be using a commercial Beryllium ICP standard solution (Scharlau), with a concentration of 1000 mg/l traceable to NIST

4.1 Proof of concept for in situ produced terrestrial krypton

We find that all zircons analysed have $^{78}Kr/^{82}Kr$ and/or $^{80}Kr/^{82}Kr$-ratios that are distinct from air (Fig. 6) and that the majority of samples form a trend that follows a hypothetical mixing line between air (Aregbe et al., 1996) and a spallogenic endmember (Gilabert et al., 2002) (Fig. 6). Neither mass-fractionation nor the addition of nucleogenic ^{80}Kr and/or ^{82}Kr can produce the main trend (Fig. 6). However, either process may account for samples deviating from the mixing line. Furthermore, all zircons contain quantifiable amounts of ^{81}Kr (Fig. 7) that, in the absence of alternative sources, must be cosmogenic. Both observations, the mixing array and the presence of ^{81}Kr demonstrate the feasibility of measuring Kr_{it} in terrestrial material.

https://doi.org/10.5194/gchron-2021-24
Preprint. Discussion started: 20 August 2021

Mass fractionation of noble gases is a common feature for samples originating from degassing magmatic systems (Kaneoka, 1980). Samples may contain residual gas from diffusive loss (enriched in heavy isotopes), or trapped gas that was fractionated during diffusion from minerals and/or degassing from melts (enriched in light isotopes). The resulting mass fractionation causes samples to plot along a path that deviates from the spallation line (Fig. 6). The samples that lie above the spallation line and to the left of the mass fractionation line (two from Mud Tank, one each from Singida and Vogtland) must contain some nucleogenic Kr; requiring bromine in the host rocks, their sources, and/or the samples themselves. Structurally there is no suitable site for bromine in the zircon lattice, so if present it is trapped in fluid or melt inclusions. Sources for kimberlites appear to be rich in halogens and in bromine (Kamenetsky et al., 2014; Burgess et al., 2009), which could explain the presence of nucleogenic Kr in some Singida and Vogtland zircons. The original melt, or source, of the Mud Tank carbonatite was rich in halogens (Currie et al., 1992), presumably containing sufficient bromine to give rise to significant nucleogenic Kr. Fractionation and the presence of nucleogenic Kr are interesting on their own account; to our knowledge natural nucleogenic Kr has not been reported before. However, for the purpose of the present study, we limit the use of the Krypton triple-isotope plot (Fig. 6) to discern samples with a simple Kr_{atm} and Kr_{it} mixture from those with complex components.

4.2 Production ratios of terrestrial cosmogenic krypton isotopes

In detail, the atmospheric - spallogenic mixing trend in $^{78}Kr/^{82}Kr$-$^{80}Kr/^{82}Kr$ space (Fig. 6) that is defined by our results is slightly steeper than the one inferred from the proton-irradiation experiments (Gilabert et al., 2002) (zircon data: 1.682±0.015 (1SD) vs. proton irradiation ≥ 49.2 g cm^{-2} shielding: 1.592±0.020 (1SD); Fig. 6). Hence, the $^{78}Kr/^{82}Kr$ and/or $^{80}Kr/^{82}Kr$ production ratios appear to be different by ~ 4% in the zircons as compared to the irradiation experiment. This small difference is unsurprising considering that in the proton irradiation experiments the 1600 MeV primary proton beam, as well as secondary protons and neutrons, produce Kr-isotopes in roughly similar proportions (Gilabert et al., 2002), whereas near the Earth surface secondary neutrons dominate (~90% at sea level (Dunai, 2010)). We take the good agreement as indication that in the mass range of ^{78}Kr to ^{82}Kr the isotopic production ratios derived from proton-irradiation experiments (Gilabert et al., 2002) are a reasonable approximation for Kr produced by spallation on Zr near the Earth's surface.

https://doi.org/10.5194/gchron-2021-24
Preprint. Discussion started: 20 August 2021

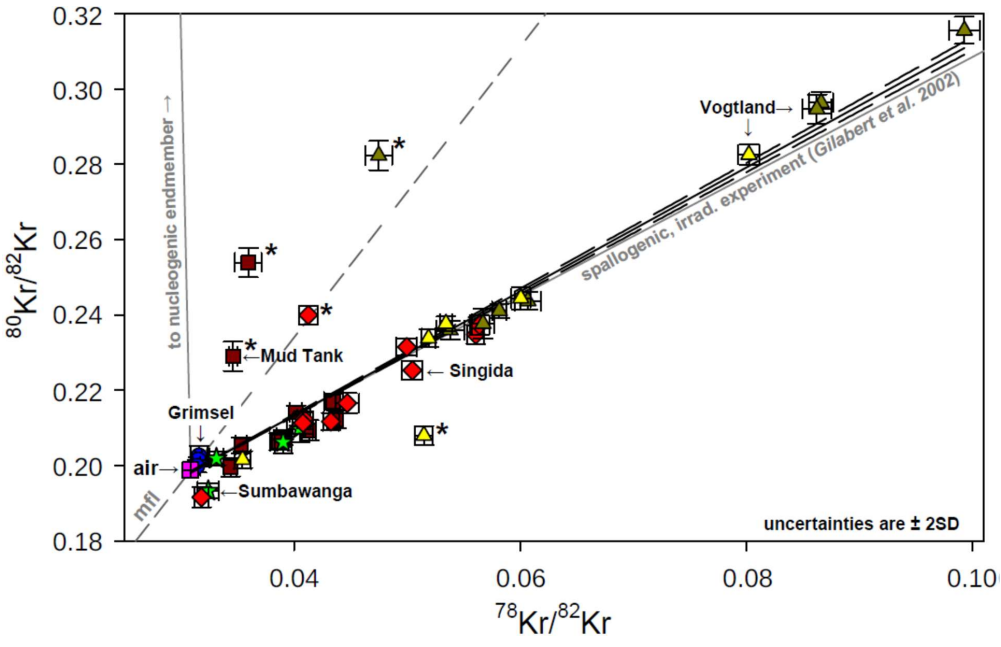

Fig. 6. Identification of krypton components and of processes fractionating krypton isotopes. Kr-data from zircons of various locations, all of which have been exposed to cosmic rays at or near the Earth's surface, form a linear trend between air (atmospheric Kr; (Aregbe et al., 1996)) and a spallogenic endmember. Several samples plot far from this trend (marked with an asterisk *). They may contain fractionated Krypton ('mfl' mass-fractionation line; (Kaneoka, 1980)) and/or nucleogenic krypton. The regression of the data (performed with regression module of SigmaPlot 14) is shown by the solid black line and excludes measurements marked with an asterisk *. The regression is forced through air. The black dashed lines are the 95% confidence intervals of the regression line. Regression of the Kr concentrations from the zircon samples indicates that the terrestrial cosmogenic endmember is slightly different to that obtained from proton irradiation experiments (solid grey line; (Gilabert et al., 2002)). Brown squares are Mud Tank carbonatite; red diamonds are for the Singida kimberlite field; green stars are Sumbawanga; blue circles are the Grimsel pass region; triangles represent Vogtland (dark yellow: samples GOEL & VOGT; yellow: samples RBM).

4.3 Cross-calibration of ^{81}Kr and ^{10}Be production rates

In samples of glacially eroded rocks from the Grimsel Pass (Switzerland) we determined concentrations of both $^{81}Kr_{it}$ in zircon and ^{10}Be in quartz (Tables 1 & 3). The resulting $^{81}Kr_{it}$(zrc)/^{10}Be(qtz) ratio is 1.545±0.045 (1SE, error weighted mean, n=3). Using a ^{10}Be production rate of 4.10±0.17 atoms g^{-1} yr^{-1} (1SE; at sea level and high latitude (SLHL) for Europe (Martin et al., 2017); LSD scaling (Lifton et al., 2014), atmospheric pressure (Uppala et al., 2005)), we derive a SLHL $^{81}Kr_{it}$ production rate of 6.33±0.32 atoms g^{-1} yr^{-1} (1SD) in zircon.

https://doi.org/10.5194/gchron-2021-24
Preprint. Discussion started: 20 August 2021

4.4 Histories of exposure and burial

Due to decay of ^{81}Kr, intermittent burial of samples lowers the measured $^{81}Kr/^{78}Kr_{it}$ ratio with respect to the production ratio; with increasing exposure time at the surface, the measured $^{81}Kr/^{78}Kr_{it}$ -ratio decreases as ^{81}Kr tends towards saturation concentrations. Hence, samples with the highest $^{81}Kr/^{78}Kr_{it}$ -ratio for a given ^{81}Kr concentration (^{81}Kr concentration is a proxy for the duration of exposure; Fig. 7) may be used to constrain the $^{81}Kr/^{78}Kr_{it}$ production ratio. Using the two samples from Mud Tank with the highest $^{81}Kr/^{78}Kr_{it}$ ratio for exposures >200 kyr (MUD-1 & MUD-11), we constrain the $^{81}Kr/^{78}Krit$ production ratio to be 1.94±0.09 (1 SE; error weighted mean). The $^{81}Kr/^{78}Kr_{it}$ production ratio derived from proton irradiation experiments is ~15% higher (for ≥ 49.2 g cm^{-2} shielding, $^{81}Kr/^{78}Kr_{it}$ = 2.30±0.02, 1SD; Table 2a of Gilabert et al. 2002). This difference may be due to unaccounted for episodes of sample burial, or the inherently different reaction pathways and energy spectra in proton experiments (Gilabert et al., 2002) as compared to the secondary neutron flux at the Earth's Surface (Lifton et al., 2014). Using either production ratio, the results for all Mud Tank zircons analysed are consistent with the $^{81}Kr_{it}$ production rate of 6.33±0.32 atoms g^{-1} yr^{-1} derived earlier and the ^{81}Kr half-life of 229±11 kyr (Baglin, 2008), assuming either a continuous exposure, a uniform erosion rate, or a complex exposure history (Fig. 7). In the following we use the $^{81}Kr/^{78}Kr_{it}$ production ratio of 1.94±0.09.

4.4.1 Glacially exhumed samples

The results of the glacially exhumed samples from the Grimsel Pass area are consistent with a post-LGM (Last Glacial Maximum) exposure under a variable and significant snow cover (Wirsig et al., 2016). Grimsel Pass $^{81}Kr/^{78}Kr_{it}$ values (Fig. 7) are consistent with the production ratio derived from the Mud Tank zircons within two standard deviations (1.94; see above), however, two of three samples are inconsistent with the experimental value (2.3, see above). Irrespective of eventual intermittent cover, samples with no exposure prior to glacial erosion history (as is inferred for Grimsel Pass area, see section 2) should exhibit $^{81}Kr/^{78}Kr_{it}$-ratios indistinguishable from the production ratio. The difference between the expected $^{81}Kr_{it}$ concentrations at Grimsel Pass (commensurate to ~13 kyr exposure (Wirsig et al., 2016)) and those measured (Fig. 7) indicate a notable amount of seasonal snow cover at our sampling locations (Wirsig et al., 2016). The quartz-vein samples used by Wirsig et al. (2016) for exposure dating were collected on steep-sided outcrops to prevent significant snow-cover; our granite samples were from near-horizontal outcrops (Fig. 3) to ensure a simple exposure geometry of our large (~10 kg; in order to recover sufficient zircon) and thick samples (10 to 15 cm).

https://doi.org/10.5194/gchron-2021-24
Preprint. Discussion started: 20 August 2021

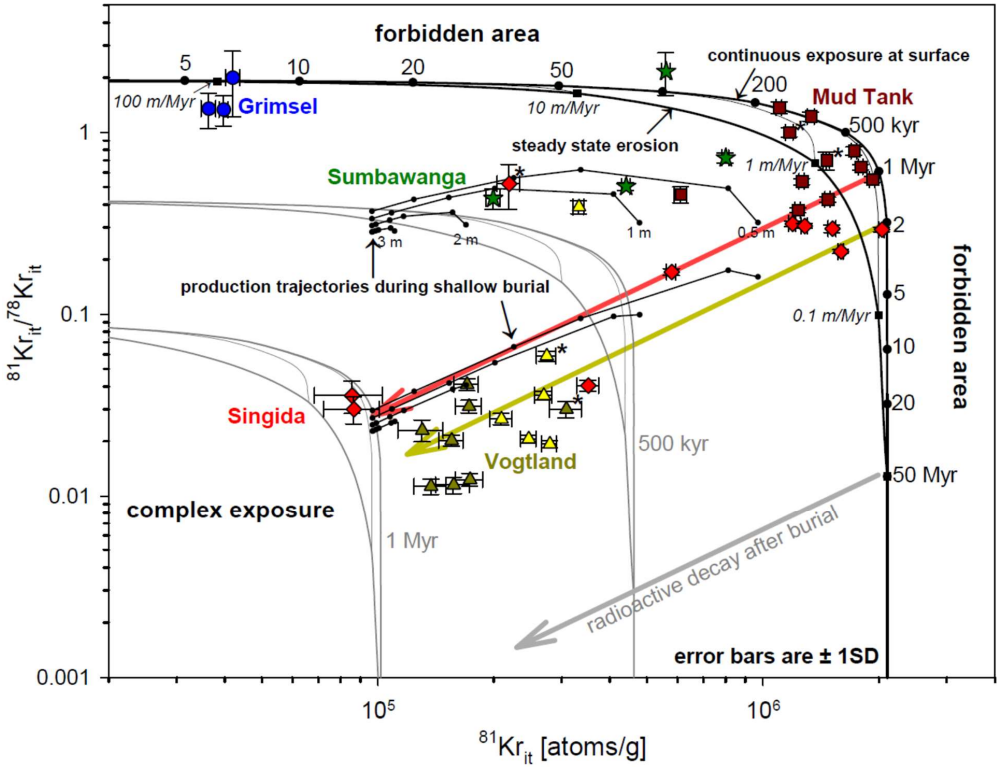

Fig. 7. Unravelling histories of exposure and burial. In a $^{81}Kr/^{78}Kr_{it}$ vs. ^{81}Kr two-isotope plot, analogous to similar diagrams used for ^{26}Al and ^{10}Be (Dunai, 2010; Lal, 1991) or ^{21}Ne and ^{10}Be (Kober et al., 2009), histories of exposure and burial can be deciphered. The spallogenic $^{81}Kr/^{78}Kr_{it}$ production ratio (1.94 ± 0.09; 1SE calculated from samples MUD-1 & MUD-11; see main text), the $^{81}Kr_{it}$ production rate (6.33 ± 0.32 atoms $g^{-1}yr^{-1}$; this study) and the ^{81}Kr half-life (229 ± 11 kyr (Baglin, 2008)) are used to define the boundaries between areas that are forbidden (no physically plausible explanation), areas that denote simple continuous exposure or steady state erosion, or complex histories that include intermittent burial. Samples that are continuously exposed at the surface may be used to test the consistency of the $^{81}Kr/^{78}Kr_{it}$ production ratio and/or $^{81}Kr_{it}$ production rate applied. Due do the decay of ^{81}Kr, the $^{81}Kr/^{78}Kr_{it}$ ratio of exposed samples decreases with increasing exposure age until the ^{81}Kr concentration eventually saturates (production rate = decay rate) after about 8 - 9 half-lives (this limit is dependent on the analytical uncertainties achieved). For exposures > 1 Myr, the $^{81}Kr_{it}/^{78}Kr_{it}$- ratio is a direct proxy for the exposure age (Marti, 1967), independent of scaling factors or shielding as long as the latter is constant through time (Marti, 1967). Upon burial the previously acquired $^{81}Kr_{it}$ inventory decays over time, allowing, in the case of a single period of deep burial, its duration to be determined. All samples are consistent with either continuous exposure at the Earth's surface, exhumation at a steady rate, or with histories that include burial after exposure ('complex exposure'). Samples marked with an asterisk (*) are those that were identified to contain fractionated and/or nucleogenic Kr (Fig. 6); results of these samples are excluded from further evaluation. The two colours used for the samples from Vogtland denote the distance they were collected downstream of their source (yellow ~5 km; dark yellow ~15 km). Symbols and colours for

https://doi.org/10.5194/gchron-2021-24
Preprint. Discussion started: 20 August 2021

samples are the same as in Figure 6. For two samples from Grimsel (GRIM-19-1 & 2) the error weighted means (1SE) of duplicate/triplicate measurements are plotted. The $^{81}Kr_{ti}$ concentrations are normalized to sea-level and high-latitude using LSD scaling (Lifton et al., 2014), and the standard atmosphere model to convert altitude into atmospheric pressure (Balco et al., 2008). The evolution trajectories shown are calculated using a $^{81}Kr_{ti}/^{78}Kr_{ti}$ production ratio of 1.94 (this study), a sea-level high-latitude $^{81}Kr_{ti}$ production rate of 6.33 (this study), the $^{81}Kr_{ti}$ half-life of 229 kyr (Baglin, 2008), and a density of 2.7 g cm^{-3} for source rocks and/or overburden. Format of diagram after Lal (1991). The two, subordinate, steady-state erosion islands bound by the grey lines give hypothetical examples of where samples would plot had they been originally exposed at the surface and then buried at a significant depth for 500 kyr, or for 1 Myr. The two sets of example production trajectories illustrate regrowth at shallower depths (i.e., 3 m, 2 m, 1 m and 0.5 m; during 500 and 1000 kyr of burial, respectively). Trajectories are vertically offset within each set for better visibility (i.e., the trajectories for the different burial depths actually originate from one point). Dots on the regrowth trajectories are for 0 yr, 10 kyr, 50 kyr, 100 kyr, 500 kyr, and 1 Myr production, respectively.

4.4.2 Sedimentary samples

The sedimentary zircon megacrysts from Australia, Tansania and Germany have the ability to record their individual (paleo-) exhumation and subsequent burial histories. Their exhumation rate is taken to be representative of the erosion rates of their former host rocks (for simplicity we assume a 2.7 g cm^{-3} density for all, which may not necessarily be the case). The simplest case is for zircons from Mud Tank (Australia), since they were collected at or near the surface in close proximity to their source rock. The sample results indicate individual exhumation rates between 1 m Myr $^{-1}$ and 0.1 m Myr $^{-1}$ and that some zircons have had a complex exposure history, with intermittent burial and/or production at shallow depths. These results are consistent with erosion rates obtained for other low-relief, post-orogenic landscapes in arid Central Australia (Struck et al., 2018b; Struck et al., 2018a) and with being sampled at or near the surface of a thin sediment cover (Australian_Vermiculite_Industries, 2013; Struck et al., 2018a).

A more complex history is implied for the zircons from the Singida peneplain (Tanzania, Mannard, 1962). The sediments of the ephemeral rivers from which they were mined commonly have a thickness of several meters; thus, samples may record extended periods of burial. The samples from the Singida form a pattern (n=9; Fig. 7) that is commensurate with exhumation rates lower than 0.1 m Myr^{-1} and continuous exposure at the surface, or burial for to up to 1 Myr. These results from the Singida diatreme field are consistent with expectations for an arid, low-relief (<50 m), long wavelength (> 10 km) landscape (Mannard, 1962; Harrison et al., 2001), notionally a relic of Cretaceous age ('African Surface'; Mannard, 1962; King, 1978; Burke et al., 2008). The notion of long-term low erosion rates is supported by the partial preservation of tuff-rings of Eocene diatremes (Mannard, 1962; Harrison et al., 2001), with the tuffs being the source-rocks of the zircons (Mannard, 1962). The erosion rates we infer from the zircons are very low (< 0.1 m Myr^{-1}), and appear to have been invariable during the last 1 Myr.

https://doi.org/10.5194/gchron-2021-24
Preprint. Discussion started: 20 August 2021

Assuming these rates apply to even longer time scales, the source of the zircons would have eroded by less than 4.5 m since the eruption of the diatreme, 44.8±0.2 Myr ago (mean U-Pb ages of zircons; n=9, 1SD; Table 2).

The basic framework for Zircons from Sumbawanga (Tanzania) is similar to Singida inasmuch as the zircons were retrieved from river sediments but the surface process rates are different. The Precambrian source rocks (Kabete et al., 2012) for zircons from Sumbawanga have experienced post Mid-Miocene uplift and tectonic segmentation as part of the Tanganyika–Rukwa–Malawi transform-segment of the East African Rift segments (Chorowicz, 2005). The resulting localized, short wavelength (1-8 km) relief is in places significant (up to 600m). The current local climate is temperate (Peel et al., 2007), rather than arid. The samples from Sumbuwanga (Fig. 7) indicate individual exhumation rates around 1 m Myr^{-1} and all but one have had a complex exposure history, with burial for up to 500 kyr and/or production at shallow depths. The order of magnitude higher erosion rates inferred for source regions of Sumbawanga zircons, as compared to Singida, are commensurate with the different tectonomorphology and climatic conditions.

The setting of the samples from the Vogtland (Germany) is distinct from the other sedimentary samples in this study as it is the only location that experienced periglacial conditions in the past (Eissmann, 2002). The area was never glaciated but was within 50 km of the ice-margins during the largest Quaternary glaciations (Eissmann, 2002). The climate is currently temperate (Bohn and Gollub, 2006; Kreklow et al., 2019). The relief is moderate, at 200 - 300 m over 2 - 3 km scale wavelengths. The zircons' source is a kimberlitic diatreme (Schmidt et al., 2013; Modalek et al., 2009) that intruded into Palaeozoic slates 71.2 ± 0.8 Myr ago (U-Pb age; Table 2). The diatreme acts as the headwaters of the drainage system investigated. The zircons from the Vogtland form a cluster (n = 13; Fig. 7) that is commensurate with a long (1 to 3 Myr) exposure at or near the surface, or exhumation at a very low rate (< 0.1 m Myr^{-1}), followed by a period of burial for 600 to 900 kyr and a recent re-emergence in the active fluvial system. Samples collected further from the source (15 vs. 5 km) appear to have longer burial histories (Fig. 7). The extremely low erosion rates inferred for exposure prior to burial (< 0.1 m Myr^{-1}) are unprecedented for temperate regions in Europe and late Quaternary erosion rates of similar moderate relief landscapes are two orders of magnitude faster (> 10 m Myr^{-1}; (Schaller et al., 2001)).

The termination of the initial, long exposure of the Vogtland zircons ~900 kyr ago, coincides with the marked climatic shifts associated with the '0.9 Ma event' (Marine Isotope Stage 22 (MIS 22); (Head and Gibbard, 2015; Mcclymont et al., 2013; Lisiecki and Raymo, 2005)) during the Mid Pleistocene Transition (MPT)(Clark et al., 2006; Head and Gibbard, 2005; Mcclymont et al., 2013). In Europe this climatic shift is associated with pronounced acceleration of river incision (Gibbard and Lewin, 2009), in

https://doi.org/10.5194/gchron-2021-24
Preprint. Discussion started: 20 August 2021

part driven by increased sediment loads from periglacial hillslope processes (Gibbard and Lewin, 2009; Goodfellow and Boelhouwers, 2013). Until the Pleistocene, low-relief landscapes dominated throughout Europe (Gibbard and Lewin, 2009; Muttoni et al., 2003; Haeuselmann et al., 2007). This stasis came to an end during the MPT (Gibbard and Lewin, 2009; Muttoni et al., 2003; Haeuselmann et al., 2007), with a step change during MIS 22 (Gibbard and Lewin, 2009; Muttoni et al., 2003). The following, first major glaciation was MIS 16 (676 to 621 kyr; (Lisiecki and Raymo, 2005; Ehlers and Gibbard, 2007)), which overlaps with the youngest burial ages of zircons in the cluster (Fig. 7). One zircon from this group may record a shorter burial, or significant post-burial production at a shallower depth.

From the external constraints on climate and landscape evolution in Europe (Gibbard and Lewin, 2009; Head and Gibbard, 2015; Mcclymont et al., 2013; Pena and Goldstein, 2014) and our results (Fig. 7) we assemble the following, preliminary, scenario. A formerly stable Plio-Pleistocene landscape (Gibbard and Lewin, 2009) is exposed for the first time to periglacial conditions during MIS 22 (Head and Gibbard, 2015; Pena and Goldstein, 2014). A functional vegetation cover is largely lost and periglacial hillslope processes accelerate sediment supply (Gibbard and Lewin, 2009; Goodfellow and Boelhouwers, 2013). The ensuing surge in sediment supply may have overwhelmed the transport capabilities of low-order catchments and consequently sediments are stored on hillslopes or in the fluvial system. In the studied case, slopes would begin to be stripped of their pre-existing regolith cover during MIS 22 and this would have been largely concluded by the end of MIS 16. The finding that the burial ages of the zircons seem to increase with distance from their source locations points to a long-term burial in fluvial sediments, rather than in colluvium proximal to their source. Analyses of additional material and locations are currently ongoing to test this preliminary scenario. For the purpose of this study, we note that Kr_{it} is suitable to illuminate (Mid-) Pleistocene histories of burial and exposure.

5 Discussion

Our results from the suite of zircon samples taken from near-surface sediments and bedrock demonstrate the feasibility and utility of Kr_{it} for Earth surface science applications. Not all Kr isotopes are equally suitable for this purpose and some aspects concerning the main target mineral, zircon, need consideration. In the following, we elucidate these topics, outline the required research to address current limitations and explore the potential of this novel tool for Earth surface sciences.

5.1 The utility of Kr-isotopes for cosmogenic applications

The utility for each of the various Kr_{it} isotopes is set by its relative abundance, the presence or absence of alternative production pathways (fissiogenic and/or nucleogenic), its half-life (where applicable) and its atmospheric abundance (^{80}Kr 2.25%; ^{82}Kr 11.6%; ^{83}Kr 11.5%; ^{84}Kr 57.0%; ^{86}Kr 17.3%; ^{78}Kr 0.35%;

https://doi.org/10.5194/gchron-2021-24
Preprint. Discussion started: 20 August 2021

^{81}Kr 0.5 ppt; (Buizert et al., 2014; Aregbe et al., 1996)), i.e., its ubiquitous general background. Specifically:

a) ^{78}Kr and ^{81}Kr are exclusively produced by cosmic rays, not by fission or nucleogenic reactions and they are the rarest Kr-isotopes in air (0.35% and 0.5 ppt in air; Fig. 1; (Buizert et al., 2014; Aregbe et al., 1996). These factors facilitate the detection and quantification of small amounts of Kr_{it}.

b) ^{80}Kr and ^{82}Kr may be produced by nucleonic reactions on Bromine, ^{79}Br(n, γ)^{80}Kr, ^{81}Br(n, γ)^{82}Kr. Reaction cross sections for thermal neutrons are 10.32 and 2.36 barn, respectively (Soppera et al., 2014). Bromine concentrations are low in silicate minerals (Ruzie-Hamilton et al., 2016; Kendrick, 2012; Teiber et al., 2015) but often not constrained. The fissiogenic production of ^{82}Kr is negligible (Fig. 1; (Jaea)). The presence of Kr_{nuc} can be verified and affected samples can be excluded from further interpretation (Fig. 6).

c) ^{83}Kr, which in meteorite studies is used as the most prominent Kr_{iet} isotope, may be produced by fission of ^{238}U (Fig. 1; (Eikenberg et al., 1993; Honda et al., 2004; Jaea)). Fissiogenic ^{83}Kr in zircon can be appreciable, since zircon is commonly enriched in uranium (particularly in comparison with meteorites) and Kr_{fis} will accumulate over the geological age of zircons (Eikenberg et al., 1993; Honda et al., 2004). Consequently, $^{83}Kr_{it}$ may not be quantified or used with the same ease as in meteorite studies.

d) Spallogenic production of ^{84}Kr and ^{86}Kr is (very) low compared to the other isotopes (Fig. 1; Gilabert et al., 2002) and their fissiogenic production rates are highest (Fig. 1; Eikenberg et al., 1993; Jaea), limiting their utility as cosmogenic nuclides.

e) Finally, the very short half-life of ^{85}Kr ($T_{½}$=10.7 yr; Lerner, 1963) renders this isotope less suited to Earth surface science applications, though there may be interesting applications that could benefit from this. However, concentrations of $^{85}Kr_{it}$ will be fiendishly low, as it approaches saturation in as little as ~50 years.

From the above (a to e) it follows that $^{78}Kr_{it}$, $^{80}Kr_{it}$, $^{81}Kr_{it}$ and $^{82}Kr_{it}$ are probably the most useful Kr_{it} isotopes for Earth surface science applications. Having three stable isotopes allows the separation of atmospheric, nucleogenic and fractionated components from cosmogenic Kr (Fig. 6). Fissiogenic production can be neglected (^{82}Kr) or excluded (^{78,80,81}Kr) for all four nuclides (Fig. 1). Finally, $^{81}Kr_{it}$ has no interference by any geochemical component (Fig. 1) and has a rather useful half-life ($T_{½}$=229±11 kyr; (Baglin, 2008)) for Earth surface science applications (Fig. 7).

Kr_{it} is unique amongst the cosmogenic nuclides in that it has one long-lived radioactive (^{81}Kr) and several suitable stable isotopes (Gilabert et al., 2002; Marti, 1967). As heavy residues of their target nuclei, Kr_{it} isotopes are not ejected from the target mineral, nor are they implanted from surrounding

https://doi.org/10.5194/gchron-2021-24
Preprint. Discussion started: 20 August 2021

material, as is the case for cosmogenic ^{3}He (Dunai, 2010; Dunai et al., 2007; Larsen et al., 2019). $^{78}Kr_{it}$ is the only stable cosmogenic nuclide that cannot be produced by processes other than cosmogenic production during the geological life-time of a rock, as its geochemical sources are gases of atmospheric composition, unaltered since the accretion of Earth (Trieloff et al., 2000). The absence of significant muogenic pathways of Kr-production from Zr-isotopes (see Sect. 1.2.2) help facilitate its use in Earth science applications.

5.2 Zircon as target mineral

Zircon is ubiquitous in igneous rocks and clastic sediments, occurring in granites as well as basalts (Grimes et al., 2007; Samson et al., 2018; Keller et al., 2017). Zircon abundance in igneous rocks is usually limited by the availability of zirconium, which has an average concentration of 82 ppm in the oceanic crust (Jenner and O'neill, 2012) and of 193 ppm in the continental crust (Taylor and Mclennan, 1985). Taking 193 ppm Zr as a guide, the average continental crust may contain 390 ppm zircon. While many granitoid rocks have zirconium/zircon concentrations close to the continental average, some might deviate significantly (Keller et al., 2017). Zircon is amongst the most weathering-resistant minerals and can survive the weathering-erosion-sedimentation-metamorphism-melting cycle of rocks (Hoskin and Schaltegger, 2003; Belousova et al., 2002).

Zircon ($ZrSiO_4$) forms a continuous mixture series with hafnon ($HfSiO_4$). In most rocks, however, the range in Hf-concentrations actually observed in zircon is small: 1.5 ± 1 wt % (Hoskin and Schaltegger, 2003; Belousova et al., 2002; Owen, 1987). Only highly evolved rocks, such as pegmatites, syenites or carbonatites, may show significantly higher Hf-concentrations (Hoskin and Schaltegger, 2003; Belousova et al., 2002). Since Hf does not contribute to Kr_{it}-production, its role in the target chemistry would need consideration (Hf 'dilutes' the Zr) when interpreting Kr_{it}- concentrations in zircons from such evolved rocks. Combined, all other impurities in zircon are well below the %-level (Hoskin and Schaltegger, 2003; Belousova et al., 2002), thus need no consideration when interpreting Kr_{it} - concentrations. Hence, in most geological contexts where zircon might be used for cosmogenic methodology, a composition of 98.5±1 % $ZrSiO_4$ may safely be assumed (Hoskin and Schaltegger, 2003; Belousova et al., 2002; Owen, 1987), without performing a chemical assay.

Retention of noble gases in zircon is very good (Honda et al., 2004; Farley, 2007). The closure temperature for Kr is between 500 and 600ºC (Honda et al., 2004). This may be a mixed blessing for some applications of Kr_{it}. On one hand, the excellent retentivity makes paleo-erosion rate studies in diagenetically altered to slightly metamorphosed rocks feasible. On the other hand, potentially incomplete resetting of the (stable) Kr_{it} by thermal diffusion in source rocks might complicate applications such as burial dating (Dunai, 2010). In any case, the retentivity of Kr_{it} under environmental

https://doi.org/10.5194/gchron-2021-24
Preprint. Discussion started: 20 August 2021

conditions will be complete in structurally intact zircons. The qualifier 'structurally intact' is pointing to the fact that radioactivity within the zircon (α-decay of U, Th, Sm) causes cumulative radiation damage over time. This can eventually lead to complete destruction of the lattice and amorphization of the material (metamictization; (Ewing et al., 2003)). This process goes hand-in-hand with an increase in volume (lowering of density by up to 17%; (Ewing et al., 2003)). Evidence from other noble gases (Guenthner et al., 2013) and other minerals (Eikenberg et al., 1993; Ragettli et al., 1994) suggests that the retentivity of Kr_{it} may be an issue for highly metamict zircons. The glassy nature of highly metamict zircons also renders them more vulnerable to weathering (Ewing et al., 2011). However, it still takes intense tropical weathering (laterization) to (partially) destroy metamict zircons (Delattre et al., 2007).

5.3 Applications in the Earth sciences

Zircon as a target material stands out in terms of weathering resistance (Hoskin and Schaltegger, 2003; Belousova et al., 2002) and retentivity for noble gases (Honda et al., 2004; Farley, 2007). This combination of characteristics complements existing cosmogenic nuclide methodology (Dunai, 2010; Marti, 1967; Granger and Riebe, 2014; Gosse and Phillips, 2001). For instance, basin-wide denudation rates (Granger and Riebe, 2014) of lateritic regoliths, which cover large tracts of the Earth surface (e.g., (Burke et al., 2008)), and quartz-free lithologies such as basalts, which are important for CO_2 draw-down (Dessert et al., 2003), may be reliably addressed without the bias that is introduced when target minerals perish during weathering (Granger and Riebe, 2014). The additional information obtained by combining cosmogenic nuclides with different half-lives is inherently available, as the relevant Kr_{it} isotopes are measured simultaneously. The important detail that ^{78}Kr has no other sources than gases of atmospheric composition and cosmogenic production, allows, in principle, the determination of paleo-erosion rates from clastic sedimentary rocks of all ages.

The results presented here provide an idea of the utility of this new tool for dating changes of process rates on the Earth surface (MPT in temperate regions), or testing their notional long-term invariance (African Surface). The ability to use stable/radionuclide pairs to track the exposure and burial history of single grains of coarse sand or fine gravel helps to achieve this. However, amalgamated, multi-grain samples for Kr_{it} are also possible and allow averaging approaches as are routinely available for other cosmogenic nuclides (Granger and Riebe, 2014), with the added benefits of an inherent stable/radionuclide pair and the unique weathering properties of zircon.

6 Conclusions

From this first study of in situ produced terrestrial krypton (Kr_{it}) we draw the following conclusions.

1. In situ produced cosmogenic krypton in terrestrial zircon can be analysed with the existing sector field mass spectrometry methodology. A high-resolution mass spectrometer aids resolving

https://doi.org/10.5194/gchron-2021-24
Preprint. Discussion started: 20 August 2021

interferences from hydrocarbons and Ar_2H^+. Likewise, a low-blank laser-extraction of Kr from zircon aids resolving small isotopic enrichments relative to atmospheric Kr.

2. ^{78}Kr, ^{80}Kr, ^{81}Kr and ^{82}Kr are the most suitable Kr-isotopes for terrestrial applications; this judgement is based on their abundance in air, the half-life of ^{81}Kr and the absence, or rarity of interfering geochemical components.
3. Cross-calibration to ^{10}Be-production in quartz ($^{81}Kr_{it}$(zrc)/^{10}Be(qtz)=1.545±0.045) yields a production rate of $^{81}Kr_{it}$ in zircon of 6.33±0.32 atoms g^{-1} yr^{-1} at sea-level and high-latitude. Our measurements indicate a terrestrial $^{81}Kr/^{78}Kr_{it}$ production ratio in zircon of 1.94±0.09 and that the air-spallogenic mixing line in $^{78}Kr/^{82}Kr$-$^{80}Kr/^{82}Kr$ space (Fig. 6) has a slope of 1.682±0.015 (uncertainties are 1SD).
4. As heavy residues of spallation, Kr_{it}-nuclei are neither implanted into zircon nor ejected from zircon. Hence, Kr_{it} production rates are not dependent on grain-size or matrix, as is the case for cosmogenic ^{3}He (Dunai, 2010; Larsen et al., 2019).
5. Interfering geochemical components and physical processes (fractionation) can be reliably identified using ^{78}Kr, ^{80}Kr and ^{82}Kr; similar to the existing methodology for cosmogenic neon (three-isotope diagram; Niedermann, 2002).
6. The combination of a stable Kr_{it}-isotope (here $^{78}Kr_{it}$) and radioactive $^{81}Kr_{it}$ ($T½$ = 229 kyr, Baglin, 2008) allows the reconstruction of complex histories of exposure and burial, similar to the existing methodology for ^{10}Be and ^{26}Al ('banana plot'; Lal, 1991). The shorter half-life of ^{81}Kr, as compared to ^{26}Al ($T½$ = 708 kyr, Nishiizumi, 2004) permits reconstructions of younger burial histories, as compared to existing methodology (i.e., combining ^{10}Be and ^{26}Al and assuming similar analytical uncertainties for equivalent exposure). The upper time-limit for resolving burial histories should be lower than 2 Myr, with the actual values of the upper and lower limits dependent on the analytical uncertainties.
7. In situations with a long, continuous exposure (> 1 Ma), ^{81}Kr-Kr-ages, which are independent of scaling, may be calculated using the existing methodology from meteoritics (Marti, 1967; Leya et al., 2015).
8. ^{78}Kr has no sources other than gases of atmospheric composition and cosmogenic production, allowing, in principle, the determination of paleo-erosion rates from clastic sedimentary rocks of all ages.

https://doi.org/10.5194/gchron-2021-24
Preprint. Discussion started: 20 August 2021

761 **Author contribution**

762 TJD conceptualized the study and designed the noble gas experiments. Investigation and formal
763 analysis of data was carried out by all authors. TJD prepared the manuscript with contributions
764 from all co-authors.

765

766 **Competing interests**:

767 The authors declare that they have no conflict of interest.

768

769 **Acknowledgements**

770 TJD would like to thank Sven Kreher (Goldmuseum Buchwald) for providing the zircons from
771 the Vogtland, sharing detailed information on the sampling sites and hands-on experience with
772 washing zircons. Many thanks to Georgina King and Peter Abbott for collecting and
773 documenting sample GRIM-1. The safe execution of the high-temperature extractions was
774 enabled by Andreas Vogt. TJD owes the integrity of the laser extraction line and probably his
775 health to these efforts, and would like to express his special thanks. TJD is very grateful to
776 Andreas Knecht (PSI) for pointing out errors in initial estimates of muon reaction probabilities.

777

https://doi.org/10.5194/gchron-2021-24
Preprint. Discussion started: 20 August 2021

References

Arblaster, J. W.: Thermodynamic Properties of Tantalum, Journal of Phase Equilibria and Diffusion, 39, 255-272, 10.1007/s11669-018-0627-2, 2018.

Aregbe, Y., Valkiers, S., Mayer, K., and DeBievre, P.: Comparative isotopic measurements on xenon and krypton, International Journal of Mass Spectrometry and Ion Processes, 153, L1-L5, 10.1016/0168-1176(96)04368-6, 1996.

Australian_Vermiculite_Industries: Mine Closure Plan Mud Tank Operation MIN 165, https://geoscience.nt.gov.au/gemis/ntgsjspui/bitstream/1/80230/3/MLS165_2014_AS_03_APPENDIX2_MCP.pdf, 2013.

Baglin, C. M.: Nuclear Data Sheets for A=81, Nuclear Data Sheets, 109, 2257-2437, 10.1016/j.nds.2008.09.001, 2008.

Balco, G.: Glacier Change and Paleoclimate Applications of Cosmogenic-Nuclide Exposure Dating, Annual Review of Earth and Planetary Sciences, 48, 21-48, 10.1146/annurev-earth-081619-052609, 2020.

Balco, G., Stone, J. O., Lifton, N. A., and Dunai, T. J.: A complete and easily accessible means of calculating surface exposure ages or erosion rates from Be-10 and Al-26 measurements, Quaternary Geochronology, 3, 174-195, 10.1016/j.quageo.2007.12.001, 2008.

Belousova, E. A., Griffin, W. L., O'Reilly, S. Y., and Fisher, N. I.: Igneous zircon: trace element composition as an indicator of source rock type, Contributions to Mineralogy and Petrology, 143, 602-622, 10.1007/s00410-002-0364-7, 2002.

Binnie, S. A., Dunai, T. J., Voronina, E., Goral, T., Heinze, S., and Dewald, A.: Separation of Be and Al for AMS using single-step column chromatography, Nuclear Instruments and Methods in Physics Research Section B: Beam Interactions with Materials and Atoms, 2015.

Binnie, S. A., Dewald, A., Heinze, S., Voronina, E., Hein, A., Wittmann, H., von Blanckenburg, F., Hetzel, R., Christl, M., Schaller, M., Leanni, L., Hippe, K., Vockenhuber, C., Ivy-Ochs, S., Maden, C., Fulop, R. H., Fink, D., Wilcken, K. M., Fujioka, T., Fabel, D., Freeman, S., Xu, S., Fifield, L. K., Akcar, N., Spiegel, C., Dunai, T. J., Aumaitre, G., Bourles, D. L., Keddadouche, K., and Team, A.: Preliminary results of CoQtz-N: A quartz reference material for terrestrial in situ cosmogenic Be-10 and Al-26 measurements, Nuclear Instruments & Methods in Physics Research Section B-Beam Interactions with Materials and Atoms, 456, 203-212, 10.1016/j.nimb.2019.04.073, 2019.

Bohn, U. and Gollub, G.: The use and application of the map of the natural vegetation of Europe with particular refernce to Germany, Biology and Environment: Proceedings of the Royal Irish Academy, 106B, 199-213, 2006.

Broadley, M. W., Barry, P. H., Bekaert, D. V., Byrne, D. J., Caracausi, A., Ballentine, C. J., and Marty, B.: Identification of chondritic krypton and xenon in Yellowstone gases and the timing of terrestrial volatile accretion, Proceedings of the National Academy of Sciences of the United States of America, 117, 13997-14004, 10.1073/pnas.2003907117, 2020.

Buizert, C., Baggenstos, D., Jiang, W., Purtschert, R., Petrenko, V. V., Lu, Z. T., Muller, P., Kuhl, T., Lee, J., Severinghaus, J. P., and Brook, E. J.: Radiometric Kr-81 dating identifies 120,000-year-old ice at Taylor Glacier, Antarctica, Proceedings of the National Academy of Sciences of the United States of America, 111, 6876-6881, 10.1073/pnas.1320329111, 2014.

Burgess, R., Cartigny, P., Harrison, D., Hobson, E., and Harris, J.: Volatile composition of microinclusions in diamonds from the Panda kimberlite, Canada: Implications for chemical and isotopic heterogeneity in the mantle, Geochimica et Cosmochimica Acta, 73, 1779-1794, https://doi.org/10.1016/j.gca.2008.12.025, 2009.

Burke, K., Gunnell, Y., Burke, K., and Gunnell, Y.: The African Erosion Surface: A Continental-Scale Synthesis of Geomorphology, Tectonics, and Environmental Change over the Past 180 Million Years,

https://doi.org/10.5194/gchron-2021-24
Preprint. Discussion started: 20 August 2021

in: The African Erosion Surface: A Continental-Scale Synthesis of Geomorphology, Tectonics, and Environmental Change over the Past 180 Million Years, Geological Society of America, 0, 10.1130/2008.1201, 2008.

Burnard, P., Zimmermann, L., and Sano, Y.: The Noble Gases as Geochemical Tracers: History and Background, in: The Noble Gases as Geochemical Tracers, edited by: Burnard, P., Springer Berlin Heidelberg, Berlin, Heidelberg, 1-15, 10.1007/978-3-642-28836-4_1, 2013.

Chorowicz, J.: The East African rift system, Journal of African Earth Sciences, 43, 379-410, https://doi.org/10.1016/j.jafrearsci.2005.07.019, 2005.

Clark, P. U., Archer, D., Pollard, D., Blum, J. D., Rial, J. A., Brovkin, V., Mix, A. C., Pisias, N. G., and Roy, M.: The middle Pleistocene transition: characteristics, mechanisms, and implications for long-term changes in atmospheric pCO2, Quaternary Science Reviews, 25, 3150-3184, 2006.

Crohn, P. W. and Moore, D. H.: The Mud Tank carbonatite, Strangways Range, Central Australia, Bmr Journal of Australian Geology & Geophysics, 9, 13-18, 1984.

Currie, K. L., Knutson, J., and Temby, P. A.: The Mud Tank carbonatite complex, Central Australia - An example of metasomatism at midcrustal levels, Contributions to Mineralogy and Petrology, 109, 326-339, 10.1007/bf00283322, 1992.

Delattre, S., Utsunomiya, S., Ewing, R. C., Boeglin, J. L., Braun, J. J., Balan, E., and Calas, G.: Dissolution of radiation-damaged zircon in lateritic soils, American Mineralogist, 92, 1978-1989, 10.2138/am.2007.2514, 2007.

Dessert, C., Dupré, B., Gaillardet, J., François, L. M., and Allègre, C. J.: Basalt weathering laws and the impact of basalt weathering on the global carbon cycle, Chemical Geology, 202, 257-273, https://doi.org/10.1016/j.chemgeo.2002.10.001, 2003.

Dewald, A., Heinze, S., Jolie, J., Zilges, A., Dunai, T., Rethemeyer, J., Melles, M., Staubwasser, M., Kuczewski, B., Richter, J., Radtke, U., von Blanckenburg, F., and Klein, M.: CologneAMS, a dedicated center for accelerator mass spectrometry in Germany, Nuclear Instruments & Methods in Physics Research Section B-Beam Interactions with Materials and Atoms, 294, 18-23, 10.1016/j.nimb.2012.04.030, 2013.

Dunai, T. J.: Cosmogenic Nuclides: Principles, concepts and applications in the Earth surface sciences, Cambridge University Press2010.

Dunai, T. J., Stuart, F. M., Pik, R., Burnard, P., and Gayer, E.: Production of He-3 in crustal rocks by cosmogenic thermal neutrons, Earth and Planetary Science Letters, 258, 228-236, 10.1016/j.espl.2007.03.031, 2007.

Ehlers, J. and Gibbard, P. L.: The extent and chronology of Cenozoic Global Glaciation, Quaternary International, 164-165, 6-20, https://doi.org/10.1016/j.quaint.2006.10.008, 2007.

Eikenberg, J., Signer, P., and Wieler, R.: U-Xe, U-Kr, and U-Pb systematics for uranium minerals and investigations of the production of nucleogenic neon and argon, Geochim. Cosmochim. Acta., 57, 1053-1069, 1993.

Eissmann, L.: Quaternary geology of eastern Germany (Saxony, Saxon–Anhalt, South Brandenburg, Thüringia), type area of the Elsterian and Saalian Stages in Europe, Quaternary Science Reviews, 21, 1275-1346, https://doi.org/10.1016/S0277-3791(01)00075-0, 2002.

Ewing, R. C., Haaker, R. F., and Lutze, W.: Leachability of Zircon as a Function of Alpha Dose, MRS Online Proceedings Library, 11, 389, 10.1557/PROC-11-389, 2011.

Ewing, R. C., Meldrum, A., Wang, L. M., Weber, W. J., and Corrales, L. R.: Radiation effects in zircon, in: Zircon, edited by: Hanchar, J. M., and Hoskin, P. W. O., Reviews in Mineralogy & Geochemistry, 387-425, 10.2113/0530387, 2003.

Farley, K. A.: He diffusion systematics in minerals: Evidence from synthetic monazite and zircon structure phosphates, Geochim. Cosmochim. Acta, 71, 4015-4052, 2007.

https://doi.org/10.5194/gchron-2021-24
Preprint. Discussion started: 20 August 2021

Gain, S. E. M., Greau, Y., Henry, H., Belousova, E., Dainis, I., Griffin, W. L., and O'Reilly, S. Y.: Mud Tank Zircon: Long-Term Evaluation of a Reference Material for U-Pb Dating, Hf-Isotope Analysis and Trace Element Analysis, Geostandards and Geoanalytical Research, 43, 339-354, 10.1111/ggr.12265, 2019.

Gerdes, A. and Zeh, A.: Zircon formation versus zircon alteration — New insights from combined U–Pb and Lu–Hf in-situ LA-ICP-MS analyses, and consequences for the interpretation of Archean zircon from the Central Zone of the Limpopo Belt, Chemical Geology, 261, 230-243, https://doi.org/10.1016/j.chemgeo.2008.03.005, 2009.

Gibbard, P. L. and Lewin, J.: River incision and terrace formation in the Late Cenozoic of Europe, Tectonophysics, 474, 41-55, https://doi.org/10.1016/j.tecto.2008.11.017, 2009.

Gilabert, E., Lavielle, B., Michel, R., Leya, I., Neumann, S., and Herpers, U.: Production of krypton and xenon isotopes in thick stony and iron targets isotropically irradiated with 1600 MeV protons, Meteoritics & Planetary Science, 37, 951-976, 10.1111/j.1945-5100.2002.tb00869.x, 2002.

Goodfellow, B. and Boelhouwers, J.: Hillslope Processes in Cold Environments : An illustration of High Latitude Hillslope Processes and Forms, in: Treatise of Geomorphology, edited by: John, F. S., Elsevier, 320-336, 2013.

Gosse, J. C. and Phillips, F. M.: Terrestrial in situ cosmogenic nuclides: theory and application, Quat. Sci. Rev., 20, 1475-1560, 2001.

Granger, D. E. and Riebe, C. S.: 7.12 - Cosmogenic Nuclides in Weathering and Erosion, in: Treatise on Geochemistry (Second Edition), edited by: Holland, H. D., and Turekian, K. K., Elsevier, Oxford, 401-436, https://doi.org/10.1016/B978-0-08-095975-7.00514-3, 2014.

Grimes, C. B., John, B. E., Kelemen, P. B., Mazdab, F. K., Wooden, J. L., Cheadle, M. J., Hanghoj, K., and Schwartz, J. J.: Trace element chemistry of zircons from oceanic crust: A method for distinguishing detrital zircon provenance, Geology, 35, 643-646, 10.1130/g23603a.1, 2007.

Guenthner, W. R., Reiners, P. W., Ketcham, R. A., Nasdala, L., and Giester, G.: Helium diffusion in natural zircon: radiation damage, anisotropy, and the interpretation of zircon (U-Th)/He thermochronology, American Journal of Science, 313, 145-198, 10.2475/03.2013.01, 2013.

Haeuselmann, P., Granger, D. E., Jeannin, P. Y., and Lauritzen, S. E.: Abrupt glacial valley incision at 0.8 Ma dated from cave deposits in Switzerland, Geology, 35, 143-146, 2007.

Harrison, T., Msuya, C. P., Murray, A. M., Jacobs, B. F., Báez, A. M., Mundil, R., and Ludwig, K. R.: Paleontological Investigations at the Eocene Locality of Mahenge in North-Central Tanzania, East Africa, in: Eocene Biodiversity: Unusual Occurrences and Rarely Sampled Habitats, edited by: Gunnell, G. F., Springer US, Boston, MA, 39-74, 10.1007/978-1-4615-1271-4_2, 2001.

Head, M. J. and Gibbard, P. L.: Early-middle Pleistocene transitions: the land-ocean evidence, Geol. Soc. Spec. Publ., 247, 1-18, 2005.

Head, M. J. and Gibbard, P. L.: Early–Middle Pleistocene transitions: Linking terrestrial and marine realms, Quaternary International, 389, 7-46, https://doi.org/10.1016/j.quaint.2015.09.042, 2015.

Hettmann, K., Siebel, W., Spiegel, C., and Reinecker, J.: Granite genesis and migmatization in the western Aar Massif, Switzerland, Neues Jahrbuch Fur Mineralogie-Abhandlungen, 186, 309-320, 10.1127/0077-7757/2009/0150, 2009.

Hoch, M., Nakata, M., and Johnson, H. L.: Vapor pressure of inorganic substances. XII. Zirconium Dioxide, J. Am. Soc., 76, 2651-2652, 1954.

Honda, M., Nutman, A. P., Bennett, V. C., and Yatsevich, I.: Radiogenic, nucleogenic and fissiogenic noble gas compositions in early Archaean magmatic zircons from Greenland, Geochemical Journal, 38, 265-269, 10.2343/geochemj.38.265, 2004.

https://doi.org/10.5194/gchron-2021-24
Preprint. Discussion started: 20 August 2021

Hoskin, P. W. O. and Schaltegger, U.: The composition of zircon and igneous and metamorphic petrogenesis, in: Zircon, edited by: Hanchar, J. M., and Hoskin, P. W. O., Reviews in Mineralogy & Geochemistry, 27-62, 10.2113/0530027, 2003.

JAEA: JENDL FP Fission Yields Data File 2011 [dataset], https://wwwndc.jaea.go.jp/cgi-bin/FPYfig, 2011.

Jenner, F. E. and O'Neill, H. S.: Analysis of 60 elements in 616 ocean floor basaltic glasses, Geochemistry Geophysics Geosystems, 13, 10.1029/2011gc004009, 2012.

Kabete, J. M., Groves, D. I., McNaughton, N. J., and Mruma, A. H.: A new tectonic and temporal framework for the Tanzanian Shield: Implications for gold metallogeny and undiscovered endowment, Ore Geology Reviews, 48, 88-124, 10.1016/j.oregeorev.2012.02.009, 2012.

Kaiser, A., Lobert, M., and Telle, R.: Thermal stability of zircon (ZrSiO4), Journal of the European Ceramic Society, 28, 2199-2211, https://doi.org/10.1016/j.jeurceramsoc.2007.12.040, 2008.

Kamenetsky, V. S., Golovin, A. V., Maas, R., Giuliani, A., Kamenetsky, M. B., and Weiss, Y.: Towards a new model for kimberlite petrogenesis: Evidence from unaltered kimberlites and mantle minerals, Earth-Science Reviews, 139, 145-167, https://doi.org/10.1016/j.earscirev.2014.09.004, 2014.

Kaneoka, I.: Rare gas isotopes and mass fractionation: an indicator of gas transport into or from a magma, Earth and Planetary Science Letters, 48, 284-292, 1980.

Keller, C. B., Boehnke, P., and Schoene, B.: Temporal variation in relative zircon abundance throughout Earth history, Geochemical Perspectives Letters, 3, 179-189, 10.7185/geochemlet.1721, 2017.

Kendrick, M. A.: High precision Cl, Br and I determinations in mineral standards using the noble gas method, Chemical Geology, 292, 116-126, 10.1016/j.chemgeo.2011.11.021, 2012.

King, L.: The geomorphology of central and southern Africa, in: Biogeography and Ecology of Southern Africa, edited by: Werger, M. J. A., Springer Netherlands, Dordrecht, 1-17, 10.1007/978-94-009-9951-0_1, 1978.

Kober, F., Ivy-Ochs, S., Zeilinger, G., Schlunegger, F., Kubik, P. W., Baur, H., and Wieler, R.: Complex multiple cosmogenic nuclide concentration and histories in the arid Rio Lluta catchment, northern Chile, Earth Surface Processes and Landforms, 34, 398-412, 10.1002/esp.1748, 2009.

Kohl, C. and Nishiizumi, K.: Chemical isolation of quartz for measurement of in-situ-produced cosmogenic nuclides, Geochimica et Cosmochimica Acta, 56, 3583-3587, 1992.

Kreklow, J., Tetzlaff, B., Kuhnt, G., and Burkhard, B.: A Rainfall Data Intercomparison Dataset of RADKLIM, RADOLAN, and Rain Gauge Data for Germany, Data, 4, 118, 2019.

Lal, D.: Cosmic ray labeling of erosion surfaces: in situ nuclide production rates and erosion models, Earth Planet. Sci. Lett., 104, 424-439, 1991.

Larsen, I. J., Farley, K. A., and Lamb, M. P.: Cosmogenic 3He production rate in ilmenite and the redistribution of spallation 3He in fine-grained minerals, Geochimica et Cosmochimica Acta, 265, 19-31, https://doi.org/10.1016/j.gca.2019.08.025, 2019.

Lerner, J.: Half-life of 85Kr, Journal of Inorganic and Nuclear Chemistry, 25, 749-757, https://doi.org/10.1016/0022-1902(63)80357-7, 1963.

Leya, I., Gilabert, E., Lavielle, B., Wiechert, U., and Wieler, R.: Production rates for cosmogenic krypton and argon isotopes in H-Chondrites with known ^{36}Cl-^{36}Ar ages, Antarct. Meteorite Res., 17, 185-199, 2004.

Leya, I., Dalcher, N., Vogel, N., Wieler, R., Caffee, M. W., Welten, K. C., and Nishiizumi, K.: Calibration of cosmogenic noble gas production based on Cl-36-Ar-36 ages. Part 2. The Kr-81-Kr dating technique, Meteoritics & Planetary Science, 50, 1863-1879, 10.1111/maps.12515, 2015.

Lifshitz, M. and Singer, P.: Nuclear excitation function and particle emission from complex nuclei following muon capture, Physical Review C, 22, 2135-2150, 10.1103/PhysRevC.22.2135, 1980.

https://doi.org/10.5194/gchron-2021-24
Preprint. Discussion started: 20 August 2021

Lifton, N., Sato, T., and Dunai, T. J.: Scaling in situ cosmogenic nuclide production rates using analytical approximations to atmospheric cosmic-ray fluxes, Earth and Planetary Science Letters, 386, 149-160, 10.1016/j.epsl.2013.10.052, 2014.

Lisiecki, L. E. and Raymo, M. E.: A Pliocene-Pleistocene stack of 57 globally distributed benthic δ18O records, Paleoceanography, 20, 2005.

Ludwig, K. R.: User's manual for Isoplot 3.75, 2012.

Mannard, G. W.: The Geology of the Singida Kimberlite Pipes, Tanganyika, Geological Sciences, McGill University, Montreal, 377 pp., 1962.

Marti, K.: Mass-spectrometric detection of cosmic-ray-produced ^{81}Kr in meteorites and possiblity of Kr-Kr dating, Physical Review Letters, 18, 264-&, 10.1103/PhysRevLett.18.264, 1967.

Marti, K., Eberhardt, P., and Geiss, J.: Spallation, fission and neutron capture anomalies in meteoritic Krypton and Xenon, Zeitschrift Fur Naturforschung Part a-Astrophysik Physik Und Physikalische Chemie, A 21, 398-+, 1966.

Martin, L. C. P., Blard, P. H., Balco, G., Lave, J., Delunel, R., Lifton, N., and Laurent, V.: The CREp program and the ICE-D production rate calibration database: A fully parameterizable and updated online tool to compute cosmic ray exposure ages, Quaternary Geochronology, 38, 25-49, 10.1016/j.quageo.2016.11.006, 2017.

Mason, B., Nelon, J. A., Muir, P., and Taylor, S. R.: The compostion of the Chassigny meteorite, Meteoritics, 11, 21-27, https://doi.org/10.1111/j.1945-5100.1976.tb00311.x, 1976.

McClymont, E. L., Sosdian, S. M., Rosell-Melé, A., and Rosenthal, Y.: Pleistocene sea-surface temperature evolution: Early cooling, delayed glacial intensification, and implications for the mid-Pleistocene climate transition, Earth-Science Reviews, 123, 173-193, https://doi.org/10.1016/j.earscirev.2013.04.006, 2013.

Measday, D. F.: The nuclear physics of muon capture, Physics Reports-Review Section of Physics Letters, 354, 243-409, 10.1016/s0370-1573(01)00012-6, 2001.

Modalek, W., Seifert, G., and Weiß, S.: Edle Zirkone aus dem Sächsischen Vogtland, Lapis, 34, 13-26, 2009.

Muttoni, G., Carcano, C., Garzanti, E., Ghielmi, M., Piccin, A., Pini, R., Rogledi, S., and Sciunnach, D.: Onset of major Pleistocene glaciations in the Alps, Geology, 31, 989-992, 10.1130/g19445.1, 2003.

Niedermann, S.: Cosmic-ray-produced noble gases in terrestrial rocks: dating tools for surface processes, Reviews in Mineralogy and Geochemistry, 47, 731-784, 2002.

Nishiizumi, K.: Preparation of 26 Al AMS standards, Nuclear Instruments and Methods in Physics Research Section B: Beam Interactions with Materials and Atoms, 223, 388-392, 2004.

Nishiizumi, K., Imamura, M., Caffee, M. W., Southon, J. R., Finkel, R. C., and McAninch, J.: Absolute calibration of Be-10 AMS standards, Nucl. Instr. Meth. Phys. Res. B, 258, 403-413, 2007.

Owen, M. R.: Hafnium content of detrital zircons, a new tool for provenance study, Journal of Sedimentary Petrology, 57, 824-830, 1987.

Peel, M. C., Finlayson, B. L., and McMahon, T. A.: Updated world map of the Köppen-Geiger climate classification, Hydrol. Earth Syst. Sci., 11, 1633-1644, 10.5194/hess-11-1633-2007, 2007.

Pena, L. D. and Goldstein, S. L.: Thermohaline circulation crisis and impacts during the mid-Pleistocene transition, Science, 345, 318-322, 10.1126/science.1249770, 2014.

Ragettli, R. A., Hebeda, E. H., Signer, P., and Wieler, R.: Uranium-xenon chronology: precise determination of l_{sf}* $^{136}Y_{sf}$ for spontaneous fission of ^{238}U, Earth Planet. Sci. Lett., 128, 653-670, 1994.

https://doi.org/10.5194/gchron-2021-24
Preprint. Discussion started: 20 August 2021

Ritter, B., Vogt, A., and Dunai, T. J.: Technical Note: Noble gas extraction procedure and performance of the Cologne Helix MC Plus multi-collector noble gas mass spectrometer for cosmogenic neon isotope analysis, Geochronology Discuss., 2021, 1-16, 10.5194/gchron-2021-11, 2021.

Ruzie-Hamilton, L., Clay, P. L., Burgess, R., Joachim, B., Ballentine, C. J., and Turner, G.: Determination of halogen abundances in terrestrial and extraterrestrial samples by the analysis of noble gases produced by neutron irradiation, Chemical Geology, 437, 77-87, 10.1016/j.chemgeo.2016.05.003, 2016.

Samson, S. D., Moecher, D. P., and Satkoski, A. M.: Inherited, enriched, heated, or recycled? Examining potential causes of Earth's most zircon fertile magmatic episode, Lithos, 314, 350-359, 10.1016/j.lithos.2018.06.015, 2018.

Schaller, M., von Blanckenburg, F., Hovius, N., and Kubik, P. W.: Large-scale erosion rates from in situ produced cosmogenic nuclides in European river sediments, Earth Planet. Sci. Lett., 188, 441-458, 2001.

Schaltegger, U. and Corfu, F.: The age and source of late Hercynian magmatism in the Central Alps - Evidence from precise U-Pb ages and initial Hf isotopes, Contributions to Mineralogy and Petrology, 111, 329-344, 10.1007/bf00311195, 1992.

Schick, H. L.: A Thermodynamic Analysis of the High-temperature Vaporization Properties of Silica, Chemical Reviews, 60, 331-362, 10.1021/cr60206a002, 1960.

Schmidt, A., Nowaczyk, N., Kampf, H., Schuller, I., Flechsig, C., and Jahr, T.: Origin of magnetic anomalies in the large Ebersbrunn diatreme, W Saxony, Germany, Bulletin of Volcanology, 75, 10.1007/s00445-013-0766-6, 2013.

Soppera, N., Bossant, M., and Dupont, E.: Janis 4: An improved version of the NEA Java-based Nuclear Date Information System, Nuclear Data Sheets, 120, 294-296, http://dx.doi.org/10.1016/j.nds.2014.07.071, 2014.

Stone, J. O., Evans, N. J., Fifield, L. K., Allan, G. L., and Cresswell, R. G.: Cosmogenic chlorine-36 production in calcite by muons, Geochim. Cosmochim. Acta, 62, 433-454, 1998.

Strashnov, I. and Gilmour, J. D.: Kr-81-Kr cosmic ray exposure ages of individual chondrules from Allegan, Meteoritics & Planetary Science, 48, 2430-2440, 10.1111/maps.12228, 2013.

Struck, M., Jansen, J. D., Fujioka, T., Codilean, A. T., Fink, D., Egholm, D. L., Fülöp, R.-H., Wilcken, K. M., and Kotevski, S.: Soil production and transport on postorogenic desert hillslopes quantified with 10Be and 26Al, GSA Bulletin, 130, 1017-1040, 10.1130/b31767.1, 2018a.

Struck, M., Jansen, J. D., Fujioka, T., Codilean, A. T., Fink, D., Fülöp, R. H., Wilcken, K. M., Price, D. M., Kotevski, S., Fifield, L. K., and Chappell, J.: Tracking the 10Be–26Al source-area signal in sediment-routing systems of arid central Australia, Earth Surf. Dynam., 6, 329-349, 10.5194/esurf-6-329-2018, 2018b.

Sturchio, N. C., Du, X., Purtschert, R., Lehmann, B. E., Sultan, M., Patterson, L. J., Lu, Z. T., Muller, P., Bigler, T., Bailey, K., O'Connor, T. P., Young, L., Lorenzo, R., Becker, R., El Alfy, Z., El Kaliouby, B., Dawood, Y., and Abdallah, A. M. A.: One million year old groundwater in the Sahara revealed by krypton-81 and chlorine-36, Geophysical Research Letters, 31, 10.1029/2003gl019234, 2004.

Taylor, S. R. and McLennan, S. M.: The continental crust: its composition and evolution, Geoscience Texts, Blackwell, Oxford1985.

Teiber, H., Scharrer, M., Marks, M. A. W., Arzamastsev, A. A., Wenzel, T., and Markl, G.: Equilibrium partitioning and subsequent re-distribution of halogens among apatite-biotite-amphibole assemblages from mantle-derived plutonic rocks: Complexities revealed, Lithos, 220, 221-237, 10.1016/j.lithos.2015.02.015, 2015.

Trieloff, M., Kunz, J., Clague, D. A., Harrison, D., and Allegre, C. J.: The nature of pristine noble gases in mantle plumes, Science, 288, 1036-1038, 10.1126/science.288.5468.1036, 2000.

https://doi.org/10.5194/gchron-2021-24
Preprint. Discussion started: 20 August 2021

Uppala, S. M., KÅllberg, P. W., Simmons, A. J., Andrae, U., Bechtold, V. D. C., Fiorino, M., Gibson, J. K., Haseler, J., Hernandez, A., Kelly, G. A., Li, X., Onogi, K., Saarinen, S., Sokka, N., Allan, R. P., Andersson, E., Arpe, K., Balmaseda, M. A., Beljaars, A. C. M., Berg, L. V. D., Bidlot, J., Bormann, N., Caires, S., Chevallier, F., Dethof, A., Dragosavac, M., Fisher, M., Fuentes, M., Hagemann, S., Hólm, E., Hoskins, B. J., Isaksen, L., Janssen, P. A. E. M., Jenne, R., Mcnally, A. P., Mahfouf, J.-F., Morcrette, J.-J., Rayner, N. A., Saunders, R. W., Simon, P., Sterl, A., Trenberth, K. E., Untch, A., Vasiljevic, D., Viterbo, P., and Woollen, J.: The ERA-40 re-analysis, Quarterly Journal of the Royal Meteorological Society, 131, 2961-3012, https://doi.org/10.1256/qj.04.176, 2005.

von Egidy, T. and Hartmann, F. J.: Average muonic coulomb capture probabilities for 65 elements, Physical Review A, 26, 2355-2360, 10.1103/PhysRevA.26.2355, 1982.

Wirsig, C., Zasadni, J., Ivy-Ochs, S., Christl, M., Kober, F., and Schluchter, C.: A deglaciation model of the Oberhasli, Switzerland, Journal of Quaternary Science, 31, 46-59, 10.1002/jqs.2831, 2016.

Woodhead, J. D. and Hergt, J. M.: A preliminary appraisal of seven natural zircon reference materials for in situ Hf isotope determination, Geostandards and Geoanalytical Research, 29, 183-195, 10.1111/j.1751-908X.2005.tb00891.x, 2005.

Wyttenbach, A., Baertschi, P., Bajo, S., Hadermann, J., Junker, K., Katcoff, S., Hermes, E. A., and Pruys, H. S.: Probabilites of muon induced nuclear-reactions involving charged-particle emission, Nuclear Physics A, 294, 278-292, 10.1016/0375-9474(78)90218-x, 1978.

Zimmermann, L., Avice, G., Blard, P.-H., Marty, B., Füri, E., and Burnard, P. G.: A new all-metal induction furnace for noble gas extraction, Chemical Geology, 480, 86-92, https://doi.org/10.1016/j.chemgeo.2017.09.018, 2018.